Optical remote sensing of large-scale water pollution caused by the Catoca Mine tailings spill

Authors:

Désirée Ruppen[1], James Runnalls[2], Raphael M. Tshimanga[3], Bernhard Wehrli[1], Daniel Odermatt[2]

[1]Institute of Science Technology and Policy, ETH Zürich, Zürich, 8092, Switzerland
[2]Department Surface Waters Research & Management, Eawag, Dübendorf, 8600, Switzerland
[3]Centre de Recherche en Ressources en Eau du Bassin du Congo, Département de Gestion des Ressources Naturelles, Université de Kinshasa, Kinshasa, DR Congo

Correspondence to: Désirée Ruppen (desiree.ruppen@istp.ethz.ch)

Abstract

Billions of tons of hazardous mine waste are stored in thousands of tailings storage facilities around the world. These impoundments represent one of the most important environmental risk factors of industrial mining, since occasional tailings spills or dam failures cause devastating impacts on human- and ecosystem health, specifically along river corridors. In this study, we developed a satellite remote sensing methodology to assess the impacts of tailings spills on water quality. We focused on the controversial incident that occurred at the Catoca diamond mine in Angola in late July 2021 and that allegedly caused important river pollution in neighboring Democratic Republic of the Congo (DR Congo) and led to public health concerns including the loss of human lives. We processed high resolution imagery acquired by ESA's Sentinel-2 satellites using the Python package Acolite for atmospheric correction and turbidity retrieval. We used a river skeletonizing algorithm to automatically extract turbidity values for the entire river system. This allowed us to track the propagation of the pollution front from the source at the Catoca mine through the Tshikapa- and the Kasaï River during more than one month and across 1400 km, until it finally dissipated after discharging into the Congo River. We further analyzed a 6-year time series of virtual stations in the Tshikapa River located up- and downstream of the effluent discharge, to compare the impacts of the tailings spill to seasonal variabilities of water quality. Turbidity values caused by the spill largely exceeded the seasonal variability in Tshikapa River in recent years. These findings confirm that the Catoca tailings spill has significantly affected water quality of the Tshikapa - and the Kasaï River with total suspended solids concentrations that were several 10-fold above drinking water standards in Lunda Norte Province, Angola and Kasaï Province, DR Congo, making severe public health impacts for residents and fish kills highly probable. We finally discuss the feasibility of transferring this methodology to other tailings dam failures that have occurred since the start of the Sentinel-2 mission in 2015. We identified available data for analyzing other incidents in China, Chile, Peru and Myanmar. Overall, our new Sentinel-2 workflow represents an opportunity to assess the large-scale impacts of pollution incidents in mining areas around the world at locations where hydrological - and water quality data is scare and monitoring capacities are limited.

1 Introduction

On 31 July 2021, local communities in the central Democratic Republic of the Congo (DR Congo) detected tons of dead fish floating on Tshikapa River whose color had turned red. The river is a lifeline to riparian communities and a tributary to the Kasaï River that flows into the Congo River. In the following days, several thousand people in the Kasaï Province requested medical attention for severe diarrhea after consuming river water and 12 people reportedly died (RTNC, 2021). About a month later, the Congolese government held a press conference confirming reports that these events were related to a tailings dam incident that occurred at the Catoca mine, one of the world's largest diamond mines located in neighboring Angola (RTNC, 2021). Subsequently, the Russian-Angolan mine operator broke the silence and published a statement in which the company accepted that a spilling incident had happened at its tailings storage facility but denied that the tailings spill had affected Tshikapa River's water quality exceptionally (Sociedade Mineira de Catoca Lda., 2021).

Unfortunately, the Catoca case is just another recent example on a long list of tailings dam incidents that have occurred in mining history. Comprehensive and up-to-date databases list over 360 tailings dam failures between 1915 and 2020 (Islam and Murakami, 2021; Rana et al., 2021). Tailings are the major waste product from ore processing and consist of an aqueous suspension of a solid phase, mainly with a grain size between silt and sand fraction. At mine sites, operators build dammed impoundments, also known as tailings storage facilities (TSF), to retain and store the tailings. Worldwide, over 18'000 active TFS's exist (Azam and Li, 2010) of which around half are located in China alone (Lepoudre, 2018). An estimated 1.2% of all tailings dams fail over a period of 100 years (Azam and Li, 2010). Globally, the frequency and the severity of the incidents are increasing, because of a growing amount of tailings to be deposited (Mudd and Boger, 2013), a lack of industry standards for TSF design, stability analysis and risk management (Clarkson and Williams, 2021) and the use of outdated dam construction methods and poor monitoring (Azam and Li, 2010).

Tailings dam incidents often have a devastating effect on the environment and humans. Severe incidents resulted in losses of hundreds of human lives and caused dramatic water pollution and biosphere damage. As recent examples, two devastating dam failures in the Minas Gerais State in Brazil have attracted worldwide media attention. The failure of the Córrego de Feijão iron mine in Brumadinho in 2019 claimed 308 human lives and was one of the most deadly tailings dam failures in history (Freitas and Da Silva, 2019). The tailings spilled high loads of turbidity, metals and nutrients into the Paraopeba River with subsequent impacts on the ecosystem. Increased ecotoxicity and fish mortality were documented even months later (Thompson et al., 2020; da Silva Souza et al., 2021). Located less than 100 km away, the Fundão tailings dam failure of the Germano iron mine in Mariana occurred in 2015. This release of an enormous amount of 60 million m^3 of metal-rich tailings left a track of devastation along more than 600 km of the river and adjacent agricultural land before discharging into the Atlantic Ocean (Rudorff et al., 2018). Several years later, local communities continue to be exposed to high concentrations of toxic metals and related health risks (Cavalheiro Paulelli et al., 2022). Not only mining ventures in the Global South are exposed to risks of such high-magnitude incidents as the dam failure in 2014 at the Mount Polley copper and gold mine in Canada has shown. The discharge of 25 million m^3 of tailings in the Quesnel River watershed resulted in more than one meter of metal-

rich sediment burying the former floodplain in the Quesnel River watershed (Hudson-Edwards et al., 2019).

As a result of severe tailings dam failures over the last two decades, new research and political initiatives focused on understanding the causes and reducing the risks of such human and environmental disasters (UNECE, 2014; Roche et al., 2017; Owen et al., 2020). Scientific studies analyzed the mechanisms of historic tailings dam failures and modelled runoff to volume relationships (Rico et al., 2008; Ghahramani et al., 2020). Other researchers provided global reviews and comprehensive databases to better understand the systematics and kinetics of the tailings dam failures (Islam and Murakami, 2021; Rana et al., 2021). Machine learning was combined with remote sensing techniques to automatically detect tailing pond structures (Li et al., 2020b). In-situ water quality measurements and geochemical analysis allowed assessing direct impact of the failures (Byrne et al., 2018; Queiroz et al., 2018; Guo et al., 2019; Hudson-Edwards et al., 2019) and the success of remediation efforts (Olías et al., 2021). Remote sensing based water quality assessments often complemented in-situ field measurements and mainly focused on turbidity (Rudorff et al., 2018; Teixeira et al., 2021) and suspended sediment concentration (Cheng et al., 2021). Other remotely-sensed products addressed resulting land cover changes of the flooded areas (Syifa et al., 2019; Moraga and Gurkan, 2020).

Specifically, the remote sensing-based assessments offer the potential to map the large-scale extent of the environmental pollution from tailings dam incidents and to establish clear evidence of the pollution sources for controversial cases. Some highly productive mines are located in forested and remote areas that are difficult to physically access due to a lack of road infrastructure. National regulators in the Global South often lack the organizational set up or the financial capacities and personnel to react to those incidents in due time and send sampling teams on the ground. Restricted access to high-security zones in some mining areas present an additional challenge for sampling and analysis efforts by independent researchers. Examples include the notoriously deadly Jade mining sites in the Hpakant area of the Kachin State in Myanmar (Global Witness, 2015), the military controlled Marange diamond fields in Chiadzwa, Mutare District, Zimbabwe (Towriss, 2013) and industrial gold mines being developed in the paramilitary-controlled Antioquia region in Columbia (Zaitch and Gómez, 2015), to mention only a few.

In the remote sensing literature, studies related to tailings dam failures primarily focus on the zone where most of the solid tailings are deposited (Ghahramani et al., 2020). Nevertheless, the mobility of the tailings depends on many factors such as their water content, precipitation intensity at the time of failure, total volume of tailings, dam height, rheological factors or downstream valley topography (Rico et al., 2008; Ghahramani et al., 2020). The solid phase of the mobilized tailings can travel far distances in a river system, while dissolved pollutants move without restriction (Simón et al., 1999; Kraus and Wiegand, 2006). The monitoring of the river water by remote sensing remains challenging because of the mixing conditions and potential methodological limitations such as image resolution (Ghahramani et al., 2020). So far, studies focusing on water quality parameters were limited to the heavily impacted zone, presenting times series of water quality parameters such as turbidity or suspended sediment load index for locations close to the source of the pollution (Rudorff et al., 2018; Cheng et al., 2021; Teixeira et al., 2021).

In our study, we present a methodological workflow that allows extracting water quality parameters of a river system based on multi-spectral Sentinel-2 satellite imagery and relate it to on-the-ground mining activity. A main practical objective of this study is to establish a solid dataset that allows clarifying whether the spill at the Catoca diamond mine in Angola was responsible for the deterioration of the water quality in the Tshikapa River and Kasaï River in neighboring DR Congo. Our approach allows the analysis of turbidity and water reflectance values over a large river reach and consequently track the pollution front. Our approach addresses to the following questions: 1) How far downstream and over which period can we track the turbidity in the river system? 2) And how strong was the impact of the Catoca tailings spill on river water quality in space and time compared to seasonal variations since 2015? After the detailed analysis of the Catoca mine spill, we look into a series of tailings dam failures that occurred over the past 6 years since Sentinel-2 imagery became available. We discuss the potential and limitations of applying our impact assessment to such incidents.

2 Study area

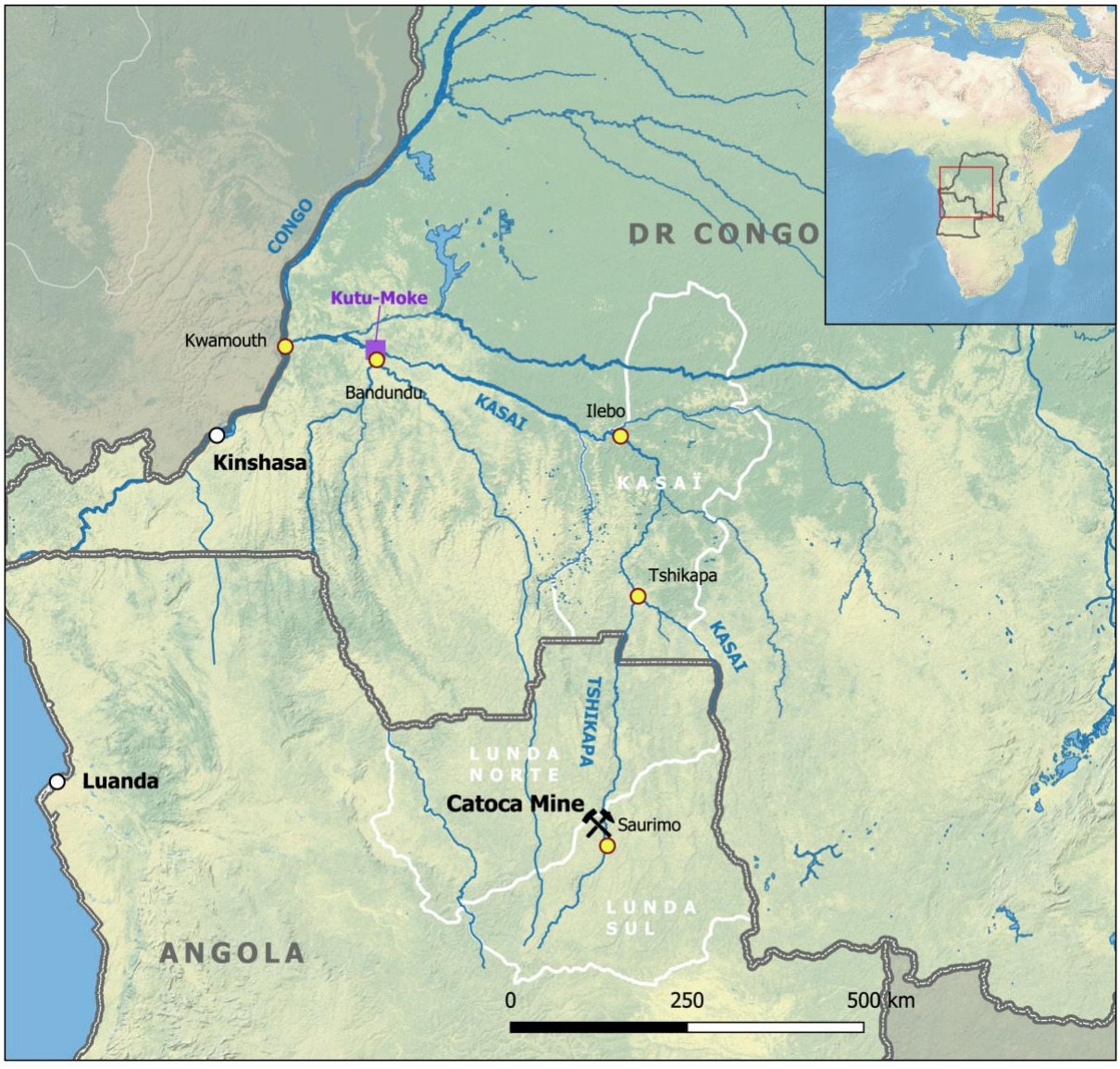

Figure 1 Map of Angola and DR Congo showing the location of the Catoca Mine and illustrating the flow of the Tshikapa River, the Kasaï River and the hydrological features of the Congo Basin. Lunda Provinces (Angola) and Kasaï Province (DR Congo) impacted by the pollution. Hydrological gauging station on Kasaï River is located at Kutu Moke. QGIS maps contain rivers and administrative boundaries from DIVA-GIS (Hijmans et al., 2018)*, places from Natural Earth* (Natural Earth, 2022) *and background layer world map* (US National Park Service, 2022)*.*

The Catoca diamond mine is located around 30 km North-northwest of Saurimo, the capital of the Lunda Sul province in the northeast of Angola (Figure 1). The mining area experiences a temperate to tropical savannah climate (Köppen, 1936; Huntley et al., 2019; Frazão et al., 2020), with a wet season from October to late April (Mendelsohn et al., 2013). With its recent production of 6.5-7 million carats of high-quality diamonds per year, the Catoca mine ranks as the world's fourth largest diamond mine by production (Cumena et al., 2019; Mining Technology, 2021). The mine is operated by the Sociedade Mineira de Catoca, a joint venture between the largest rough diamond producer in the world, Russian state-owned Alrosa (with a share of 41%), the Angolan Government-owned Endiama (32.8%) and the Chinese LL international Holding B.V. (18%) (Alrosa, 2021).

In Catoca, the ore is extracted at an open pit mine, processed on site and the tailings are deposited in a TSF with a surface of around 11.5 km^2 (Figure 2a). The impoundment stores around 35 Mio m^3 of tailings (Santos, 2021). The spillover from the dam is discharged into the small Lova River, a tributary of the Tshikapa River (spelled Chicapa on the Angolan side) which crosses the area in South to North direction. Discharge data of the Tshikapa River were not available, however, a hydroelectric plant under construction some 20 km downstream of Saurimo (Da Cruz, 2016; Gupta and Shankar, 2022) has a spillway designed for a maximum flow of 467 $m^3 s^{-1}$ (COBA Group, 2015).

The Tshikapa River has its source in the Angolan highlands some 200 km southwest of Saurimo. After passing the Catoca mining area, the Tshikapa River meanders northwards for some 360 km across the Lunda Norte Province where several other industrial diamond mines are operating in vicinity to its course (S&P Global Market Intelligence, 2021). In addition, thousands of *garimpeiros* extract alluvial diamonds in shallow pits or use boats and diving equipment to mine the diamonds from the riverbed (PAC, 2004; AMDC, 2017; Cumena et al., 2019). After setting the border with neighboring DR Congo for around 60 km, the Tshikapa River crosses into the Kasaï Province of DR Congo where it joins the Kasaï River at the town of Tshikapa after another 80 km of flow. The Kasaï River is a main tributary to the Congo River and its sub-catchment drains one fourth of the surface of the 3.7 Mio km^2 large Congo Basin (Mushi et al., 2022). From Tshikapa Town the Kasaï River flows for around 880 km north- and then westwards where it passes the towns of Ilebo and Bandundu before finally discharging into the Congo River at Kwamouth.

2.1 Runoff and turbidity

In the Congo Basin, runoff data and water quality measurements are scarce. Hydrological modelling studies of the Congo Basin still use historical gauging data from colonial times (Tshimanga, 2012; Munzimi, 2019). For the Kasaï River, two gauging stations are included in the international database of

the Global Run Off Data Centre (GRDC) with data collected between 1932 to 1959 (BFG, 2022). One station was located at Ilebo where the Kasaï River had a mean monthly discharge of 2114 $m^3 s^{-1}$ in the historical dataset (Munzimi, 2019). The second gauging station was located at Kutu-Moke (Figure 1). It was recently renewed with international donor support and is currently managed by the Congolese water research institute *Centre de Recherche en Ressources en Eau du Bassin du Congo* (CRREBaC). Since September 2017 it is an operational hydrological- and sediment monitoring station where turbidity measurements and sediment samples are taken and river discharge is measured. Between June 2018 and August 2019 the turbidity sensor recorded a median nephelometric front scatter turbidity [FNU] of 124.7, a mean of 281.5 FNU and a standard deviation of 341.7 FNU (Mushi et al., 2022). From August 2018 to August 2019, suspended sediment concentration showed a median of 476.9 mg L^{-1}, mean of 517.8 mg L^{-1} and a standard deviation of 324.7 mg L^{-1}. For the same period of time the discharge of the Kasaï River varied between a minimum in August of 4510 $m^3 s^{-1}$ and a maximum of 12185 $m^3 s^{-1}$ in March 2019 (Mushi et al., 2022).

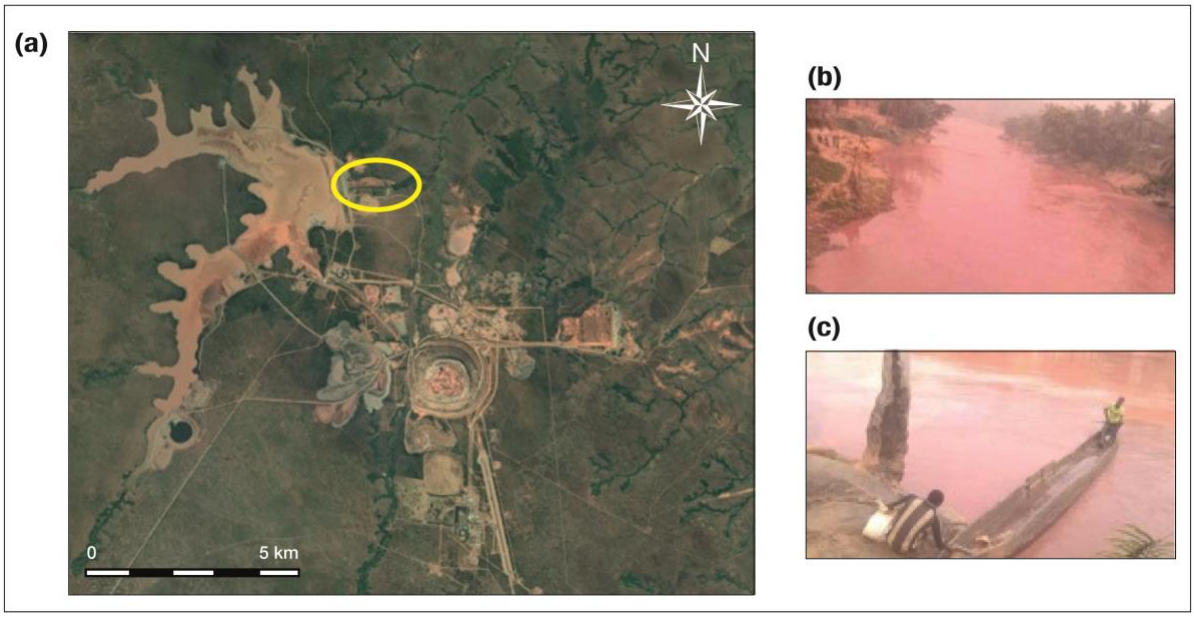

Figure 2 (a) Satellite Image of the Catoca Mine, Angola. Open pit extraction in the center and tailings storage facility in the West of image. Debris flow caused by tailings spill highlighted with yellow circle Google Earth Pro 7.3.4.8248 (August 01, 2021). 09° 24' 15.15"S, 20° 18' 06.42"E, Eye alt 15.76 km. Maxar Technologies 2022. https://www.earth.google.com [March 14, 2022]. (b) & (c) Kasaï River close to Tshikapa Town showing red coloring in early August 2021 (Picture credits: Stany Frank).

2.2 Chronology of the pollution incident

Following accounts of concerned residents, the Angolan media reported in early August 2021 the pollution of the Lova River in Lunda Sul Province, the stream into which the Catoca diamond mine discharges its effluents. The Catoca mine management confirmed to the local authorities that on 27 July 2021, the drainage system of their tailings pond had burst, causing the pollution of the river (Figure 2B,C) and adjacent areas (TPA, 2021b). Mid of August 2021, CRREBaC published a leaflet reporting important changes in water quality and vast fish kills in the Tshikapa River in the DR Congo (CRREBac, 2021). The consultancy company Visio Terra visually analyzed satellite imagery and identified signs of

water pollution as early as 25 July that they related to a number of mine sites in Angola as being the source of the pollution (Sentinel Vision and Visio Terra, 2021).

Roughly 1.5 months after the incident in early September 2021, the Congolese Government held a press conference in the capital Kinshasa with the Vice- Premier Minister and Minister of the Environment as main speaker (RTNC, 2021). The minister reported that from 26 July residents noticed changes in color of the river water and on 31 July 2021 tons of fish and two hippopotamuses were found dead in the Tshikapa River in the Kasaï Province. The minister mentioned that a research team took samples with nickel and iron values above thresholds but she presented no data. The minister added that 9863 people were affected by the incident in the sanitation zone of Bangalubaka, Territory of Ilebo, Kasaï Province, with 4502 reported cases of diarrhea and 12 deaths (RTNC, 2021). She underlined that the pollution incident in the DR Congo was linked to a mining accident in Angola, more precisely at the diamond mine of Catoca, and mentioned ongoing diplomatic procedures (RTNC, 2021). The pollution of the Tshikapa River attracted vast media attention and was covered internationally (Holland and Reid, 2021; Neto and Maclean, 2021; VoA Português, 2021a).

A day after the Congolese press conference, the Catoca mining company released a statement on their website. A rupture in the pipeline that works as a flood spillway was acknowledged. The statement added that *"the tailings basin contains only mixtures of natural rocks, such as sand and clay, and the composition of matter corresponds approximately to the mud flows in the rainy season and does not contain external chemical components, which allows us to state that this situation does not represent risk to the affected populations."* (Sociedade Mineira de Catoca Lda., 2021). In several interviews Angolan Provincial government representatives denied that the spill incident had deteriorated water quality in the Lova or Tshikapa Rivers in an unexceptional way and refused that it had caused any health issues to communities neither on the Angolan nor the Congolese side (Santos, 2021; TPA, 2021c, 2021a). The chief of the Provincial Environment Department of Lunda Sul province also highlighted that *"the Chicapa and Lova Rivers already have a history of pollution caused by artisanal diamond mining … There have always been abnormal turbidity levels."* (TPA, 2021c) .

In summary, two events were not contested, the occurrence of a tailings spill at Catoca mine, and the subsequent fish kills. However, the timing of the incident and the causal link between the spill and the deterioration of the water quality remain controversial. This raises the question, whether remote sensing could provide additional evidence.

3 Remote sensing data and methodology

We base our analysis on high-resolution optical imagery acquired by the Multispectral Imager (MSI) on the Sentinel-2 (S-2) satellite of the European Space Agency's (ESA). The constellation comprises two polar-orbiting satellites (S-2A and S-2B) in the same sun-synchronous orbit phased at 180° to each other. This allows high revisit times of 5 days at the equator (ESA, 2021). The imagery contains 13 bands in the visible and near-infrared (NIR) wavelengths with resolutions of 10, 20 or 60 meters, which are provided in 100 x 100 km tiles. Our region of interest extends across 14 such tiles (Table 1). Between the Catoca mining area and the Congolese town Ilebo, the Tshikapa River and subsequently

the Kasaï River run in South to North direction for 900 km, which falls within a single MSI swath with full coverage every 5 days. By contrast, the Kasaï River between Tshikapa and Kwamouth runs East to West, with a longitudinal extension that is roughly twice the MSI's swath (Figure 3) and full coverage takes three days within the five-day revisit interval. We used the Python package Sencast to download, process and visualize S-2 data (https://gitlab.com/eawag-rs/sencast). In total, we downloaded about 400 S-2 L1C top-of-atmosphere-reflectance datasets (ESA, 2018) from a Copernicus Data and Information Access Service (www.creodias.eu). They include the full region of interest during the dam spill, plus all observations of the Catoca mine perimeter acquired since the launch of S-2A in June 2015.

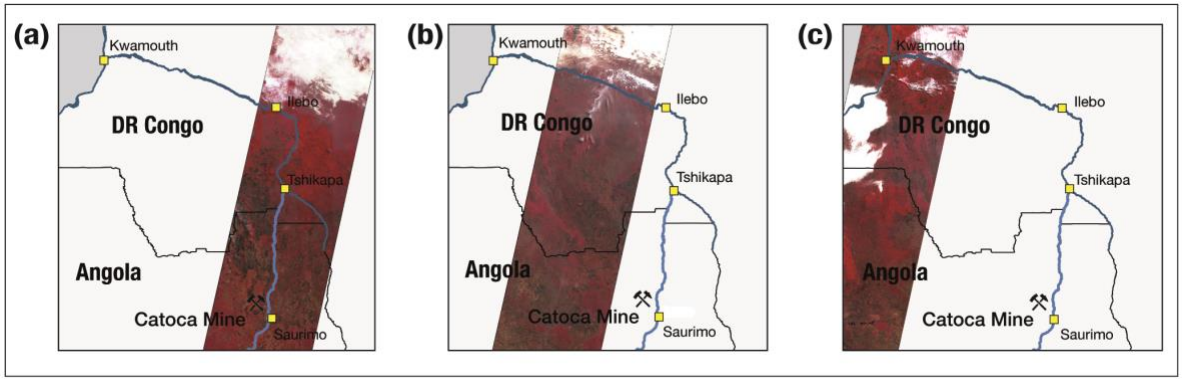

Figure 3 Three MSI swath widths (290 km) were necessery to cover the region of interest: (a) Swath covering the Tshikapa- and the Kasaï River flowing from Catoca Mine to Ilebo (b) Swath that covers the Kasaï River between Ilebo and Bandundu and (c) The Kasaï River between Bandundu and Kwamouth. Swath in false color composite from Sinergise (2022) *for 20 July, 23 July and 21 July 2021, respectively. Background map showing locations and rivers of interest, adapted from Figure 1.*

To remove atmospheric effects from the radiance signal and convert it to surface reflectance, atmospheric correction was done using release 20211124.0 of the Python package Acolite (Vanhellemont, 2019, 2020) as a subroutine in Sencast. Acolite further allowed us to identify water surfaces by performing non-water pixel masking. Acolite was found to perform best in very turbid optical water types (Pahlevan et al., 2021), and its recommended Dark Spectrum Fitting (DSF) method is useful for atmospheric correction over extremely turbid water, in which case atmospheric optical thickness (AOT) is estimated from dark pixels in the water body's adjacency. Acolite masks non-water pixels with a maximum threshold in L1C top-of-atmosphere reflectance (ρ_t). We used the default 1610 nm band for this task. Due to extraordinarily high aquatic backscattering, the default threshold of $\rho_{t,1610}$=0.0215 is consistently exceeded in S-2 data of the Tshikapa- and Kasaï Rivers after the spill incident, despite low atmospheric turbidity. We therefore applied a relaxed masking threshold of $\rho_{t,1610}$=0.09 to all data, and verified visually that both water courses were still adequately masked in data acquired prior to the spill. Likewise, we adjusted the cirrus cloud masking threshold of Acolite, by $\rho_{t,1373}$=0.005, to $\rho_{t,1373}$=0.009. The default mask smoothing was disabled.

In order to correct atmospheric effects, Acolite first corrects ρ_t with regards to atmospheric gas transmittance and the diffuse sky reflectance at the air-water interface. Then, Acolite's DSF algorithm fits an Ordinary Least Squares (OLS) regression through the darkest pixels of each spectral band corrected in such manner (Vanhellemont and Ruddick, 2018). The OLS intercepts yield a representative dark spectrum, which is used to select a spectral band and aerosol model for the estimation of AOT at 550 nm from a Look-Up-Table (LUT). The same LUT accounts for path reflectance, atmospheric

transmittance and spherical atmospheric albedo when calculating water-leaving reflectance (ρ_w) from path-corrected reflectance. We used Acolite's default configuration, but changed *luts_reduce_dimensions=False* to avoid the 1 m^{-1} AOT limit of the reduced LUT. We harmonized the choice of aerosol models for spatial analyses along the river network, where switching aerosol models lead to stitching artefacts between subsets. Maritime aerosols were chosen by Acolite in 120 of 132 such subsets. We therefore forced the use of maritime aerosols also for the remaining twelve tiles, by using luts=ACOLITE-LUT-202110-MOD2. Sun glint correction was not applied.

Aquatic turbidity is closely related to remote sensing reflectance in red and Near-Infrared (NIR) spectral bands, and the higher the turbidity, the larger the preferred wavelength (Nechad et al., 2009; Odermatt et al., 2012). Dogliotti and colleagues developed a switching algorithm using in-situ measurements in the range 1-2000 FNU (Dogliotti et al., 2015). It retrieves low to moderate turbidity using an arithmetic equation for MODIS' 645 nm band, while moderate to high turbidity is retrieved using an analogous equation for MODIS' 859 nm band. The Acolite manual (Vanhellemont, 2021) reports coefficients that Bouchra Nechad calculated in 2016 for using these two arithmetic equations with the 10 m S-2 bands at 665 and 833 nm (Eq. 1, Eq. 2):

Eq 1:

$$T_{665} = \frac{366.14\,\rho_{w,665}}{1 - \rho_{w,665}/0.19563}$$

Eq 2:

$$T_{833} = \frac{1913.65\,\rho_{w,833}}{1 - \rho_{w,833}/0.1913}$$

which we adopted for use in Acolite's implementation of the switching algorithm by Dogliotti et al. (2015) according to Eq. 3:

Eq 3:

$$T(\rho_{w,665} \leq 0.05) = T_{665}$$

$$T\left(\rho_{w,665} \geq 0.07\right) = T_{833}$$

$$T(0.05 < \rho_{w,665} < 0.07) = (1 - w)\,T_{665} + w \cdot T_{833}$$

It is important to note that both arithmetic equations behave asymptotically when the respective ρ_w approaches the coefficient in the denominator. For Eq. 1 this property is ineffective due to the switching mechanism. But the asymptote at $\rho_w(833) = 0.1913$ represents a saturation limitation of the algorithm, given that this threshold is reached and exceeded on many occasions after the Catoca dam spill, and under cloud and cirrus free conditions. Using MSI's reference signal-to-noise ratio of 174 in band 8 (ESA, 2015), we estimate that the noise equivalent error due to this saturation increases from 2% at 1000 FNU to 10% at 5800 FNU. We therefore define a calibrated (0-2000 FNU), an extrapolated (2000-5800 FNU) and a saturated (>5800 FNU) retrieval range, and we mask all values obtained in the

saturated range, as well as values with $\rho_w(833) > 0.1913$ that yield negative turbidity according to Eq. 2. All estimates masked in such manner are treated as 5800 FNU for further analyses and visualization.

We used the processing pipeline described above to produce turbidity maps covering the Catoca spill area and the river flow path for specific dates related to the incident. We considered satellite imagery that was sensed shortly before the incident and during a month after the incident. The swath coverage of the Sentinel-2 satellites determined the specific sensing dates along the river path (see Figure 3). Cloud coverage restricted automatized pixel extraction on several sensing dates. Accordingly, we were able to generate turbidity maps for the different river sections for one satellite image sensed prior to the incident, namely on 20 July 2021, and for eight dates after the incident between 25 July to 30 August 2021 (details see Table 1). To produce longitudinal sections of turbidity, we required an accurate centerline (one-pixel-wide) of the river system. But the width of the Tshikapa River is at the lowest limit of MSI's resolution. Which means that mixed pixels from a relatively tolerant land-water mask and uncertainties in geolocation impedes the use of a static river pixel grid. Alternatively, there are a number of published algorithms for extracting a river network from satellite images for example RivWidth (Pavelsky and Smith, 2008) and NRBC method (Zeng et al., 2015). Most involve generating a Boolean map of river pixels, applying a skeletonization or thinning algorithm and then pruning any undesirable branches. For this study, we use the Acolite water classification map to define water pixels in the processed image. By overlaying the Boolean water matrix with a buffer zone around a rough vector river path that we produced, we could extract a Boolean matrix of river pixels. Since the algorithm determines the shortest route, it occasionally left the main river path and followed a small side branch of the river. In such cases, we manually removed pixels from the river matrix which allowed us to block the side branch and force the algorithm to follow the main river path. We then thinned the river matrix using the scikit-image (Van der Walt et al., 2014) and implemented Zhang and Suen's thinning method (Zhang and Suen, 1984). The output river skeleton was abstracted to nodes and edges and the shortest path between the start and end pixels was calculated with the NetworkX implementation (NetworkX, 2022) of Dijkstra's algorithm (Dijkstra, 1959). For networks with disconnected start and end nodes, a high-cost edge was introduced between adjacent non-connected nodes. The river skeletons were loaded onto the corresponding Level-2 imagery. For each pixel coordinate of the river skeleton, the turbidity value was extracted from the Level-2 product by aggregating the median based on a 3x3 pixel filter with the given pixel at the center. This filter was used to account for potential mixed pixels along the skeleton, assuming that a minor fraction of the 3x3 pixels are subject to additive (e.g. soil, vegetation) or reductive effects (e.g. shading) at sub-pixel scale. The complete processing algorithm is available on GitHub (https://github.com/JamesRunnalls/catoca-tailings-failure).

We started the automatized extraction of the water turbidity in the Tshikapa River around 40 km upstream of the inflow to the Lova River. The pixel extraction followed the course of the Tshikapa River for 540 km to the confluence with the Kasaï River near the Congolese town Tshikapa. Automatized pixel extraction was successful for up to 650 km of flow for 20 July 2021 and up to 130 km less for three dates after the tailings spill, namely 25 July, 30 July, 04 August, since extraction ceased towards north due to cloud coverage. For the rest of August 2021, automatized image processing was hindered due to high cumulus cloud coverage or haze on the entire MSI swath. On the second MSI swath to the West, we successfully extracted 17 August and 22 August in this middle section between the towns of

Ilebo and Bandundu (Table 1). We also present the values we extracted in a third section covering the last 222 km Kasaï River before reaching the mouth of the Congo River for three dates showing the pollution front (10 August, 15 August, 25 August) and a last date after the pollution front has disappeared again (30 August 2021). The turbidity values were smoothed with a moving average (median) over 300-pixel stretches, in order to remove small-scale variability related to both the actual target parameter (e.g. resuspension) as well as its retrieval uncertainties.

Table 1 List of Sentinel-2 tiles extracted for given dates, MSI swaths relate to Figure 3..

MSI swath	Sentinel-2 tiles	River distance covered	Extracted dates [2021]
A	34 LDQ, 34 LDR, 34 MDS, 34MDT, 34MDU, 34MDV, 34MEV, 34 MDA	Tshikapa River at mine level to Ilebo	20 July, 25 July, 30 July, 04 August
B	34 MCA, 34MBA, 34MBB	Ilebo to Bandundu	17 August, 22 August
C	33 MZS, 33MYS, 33MXS	Bandundu to Kwamouth	10 August, 15 August, 25 August, 30 August

To compare the different river skeletons on a same longitudinal section, we used the river skeleton of the first day which was sensed of the respective MSI swath and compiled for each river skeleton of the other dates a nearest neighbor matrix using the QGIS geographic information system (QGIS Development Team, 2022). For the first 650 km, the river skeletons of 25 July, 30 July and 04 August were projected onto the river skeleton of 20 July 2021. For the section between Ilebo and Bandundu, the river skeleton of 22 August was projected onto the one of 17 August. For the section at the mouth of the Kasaï River, the river skeletons of 15, 25 and 30 August where projected on the river skeleton of 10 August 2021. The distances between the pixels of the reference three river skeletons were calculated using the QGIS field calculator and summed up to display the river flow distance. We used R for data analysis (R Core Team, 2018) and plotted figures using ggplot 2 (Wickham et al., 2019). The Sentinel-Hub EO browser (Sinergise, 2022) was used to visually inspect the Sentinel-2 imagery of the year 2021 and localize the pollution front in true color composite (B4, B3, B2) or in false color composite (B8, B4, B3).

To discuss potential impacts on human and ecosystem health, we used the formula presented by Rasmussen and colleagues that established a linear correlation between suspended solids concentration (SSC) and turbidity values [FNU] for the Little Arkansas River near Sedgwick, Kansas (Rasmussen et al., 2009).

Eq 4:

$$SSC\ [mg\ L^{-1}] = 1.39 * Turbidity[FNU\ ]^{0.943}$$

4 Results

In the following, we present the propagation of the pollution front in the Tshikapa and the Kasaï River, as well as a time series of two virtual stations in the Tshikapa River close to the Catoca mine. The

Sentinel-2 image of 20 July was the last one documenting the situation prior to the tailings spill. On the next image sensed five days later on 25 July 2021, a debris deposit of 16.75 ha is visible for the first time adjacent to the tailings dam (see Figure 2a). The dam wall itself and the extent of the tailings storage facility appear unaltered. The Lova River that receives the mine effluent has a brownish color, which reflects high turbidity levels. The Tshikapa River, which is blue upstream, changes its color to brown after of the confluence with the Lova River. The color change in Tshikapa River after the inlet of the Lova River was not discernable 5 days earlier. (Processed images available on GitHub).

4.1 Propagation of pollution front

Prior to the incident, turbidity over the entire river stretch showed an average of 127 FNU and maximum values of 272 FNU in the 300-pixel smoothed median (Figure 4). To explain the turbidity changes, we used high-resolution satellite imagery using Google Earth Pro (Google LLC., 2021) to map mines that operate close to the river course (S&P Global Market Intelligence, 2021) and plotted them with respect to the river course (Suppl.-Table 2 in Appendix). The effluent of the Catoca mine that joins the Tshikapa at km 40 of the longitudinal profile causes no notable turbidity change on the image of 20 July 2021. The first increase is encountered another 24 km downstream where numerous ASM pits are located along the flow path. Here, artisanal miners extract the shallow alluvial deposit on the shores and thereby enhance turbidity. This phenomenon is well known from other ASM contexts (de Lucia Lobo et al., 2017). The turbidity increases nearly 10-fold after the Tshikapa passes the Canvuri and the Camatchia -Camagico mine that are located close to each other. The latter visibly discharges effluent with high sediment load to the Tshikapa River. The turbidity values consequently decrease until the Tshikapa River passes the next extraction site of the Calonda mine, followed by the city of Calonda, and the Yetwene Mine that all discharge effluents into the river. The Tshikapa River joins the Kasaï River at the Congolese town of Tshikapa. At this point, the turbidity decreased close to 100 FNU as the larger Kasaï River dilutes the concentration of suspended sediments carried by the 5-10 times smaller Tshikapa.

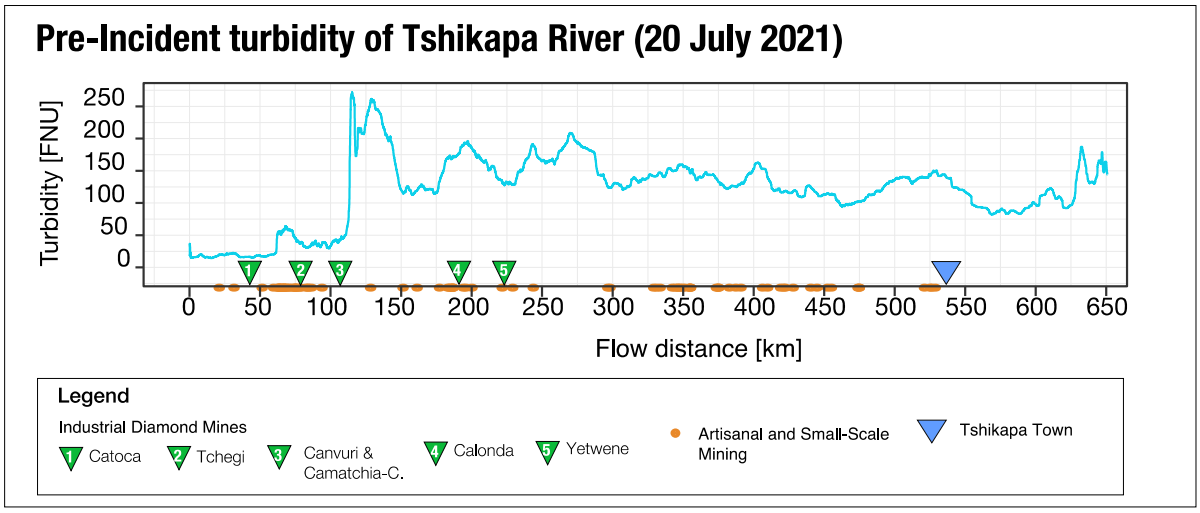

Figure 4 Pre-incident turbidity [FNU] along the Tshikapa River [km]. Values displayed for 650 km starting 40 km upstream of the Catoca Mine.

Although mining activities affect the turbidity on 20 July 2021, observations after the spill incident reveal a stark contrast (Figure 5). In the scenes from 25 July, 30 July and 04 August that follow the spill, we observe a very abrupt and steep turbidity increase where the Lova River discharges into the Tshikapa River. The water loaded with dam failure debris saturates the turbidity retrieval algorithm (shown as 5800 FNU) consistently and across large areas. We cannot robustly quantify turbidity at such levels, but conservatively estimate an increase that is in the order of 50- to 100-fold the median prior to the incident. On 25 July, the turbidity values remain at the saturation level for 38 km before rapidly decreasing to pre-incident levels. On 30 July the turbidity remains at saturation level for 306 km before decreasing more slowly and finally reaching pre-incident level after another 159 km of flow. For 4 August, turbidity saturation extends over a distance of 440 km before starting to decrease. The duration of the leaking at the Lova mouth cannot be estimated directly, because it extended into the wet season, and cloud-free images are lacking. On 4 August, the pollution front was visually identified through semi-transparent clouds, 201 km North of Tshikapa, at 696 km from the mouth of the Lova River. But no valid pixels are available from Acolite due to the clouds.

In the middle section of the Kasaï River between Ilebo and Bandundu the cloud coverage was high end July and early August. We visually localized the pollution front in the center of this middle section on 7 August. The first date for which it was possible to extract pixels was the 17 August on which turbidity levels were increased with an average of 308 FNU. Five days later, the turbidity was 5-fold lower at 96 FNU, which is presumably the baseline in this section.

In the last section at the mouth of the Kasaï River, we observed the arrival of the pollution front on 10 August. Five days later, on 15 August pollution levels reached a maximum of 320 FNU. Shortly before and a dozen kilometers downstream of the sampling station Kutu Moke (1250 km flow distance), three main tributaries, the Kwango-, the Kwilu and the Fimi River join the Kasaï (Mushi et al., 2022). Here, the pollution signal decreased to a median of 125 FNU and quickly dropped to levels around 20 FNU when the Kasaï River mixed with water from the Congo River at the town of Kwamouth. Similar patterns were observed on 25 August for the last 100 km. However, median levels dropped by 50% and on 30 August, pre-incident levels of a median of 20 FNU were reached again.

The pollution front was localized on five dates which allowed us to calculate the velocity at which the pollution propagated. These propagation velocities reached for median and average the same value of 0.81 m s^{-1} (Figure 6 & Suppl.-Table 3 in Appendix). We conclude that the tailings spill started at around midday of 24 July 2021 and the pollution front arrived at the Congo River on 13 August in the early afternoon. The Sentinel-2 image of 15 August confirms that the pollution had reached the Congo River and that the reddish coloring of the incoming Kasaï River water only dissipated after another 20 km downstream in the direction of the Congolese capital Kinshasa.

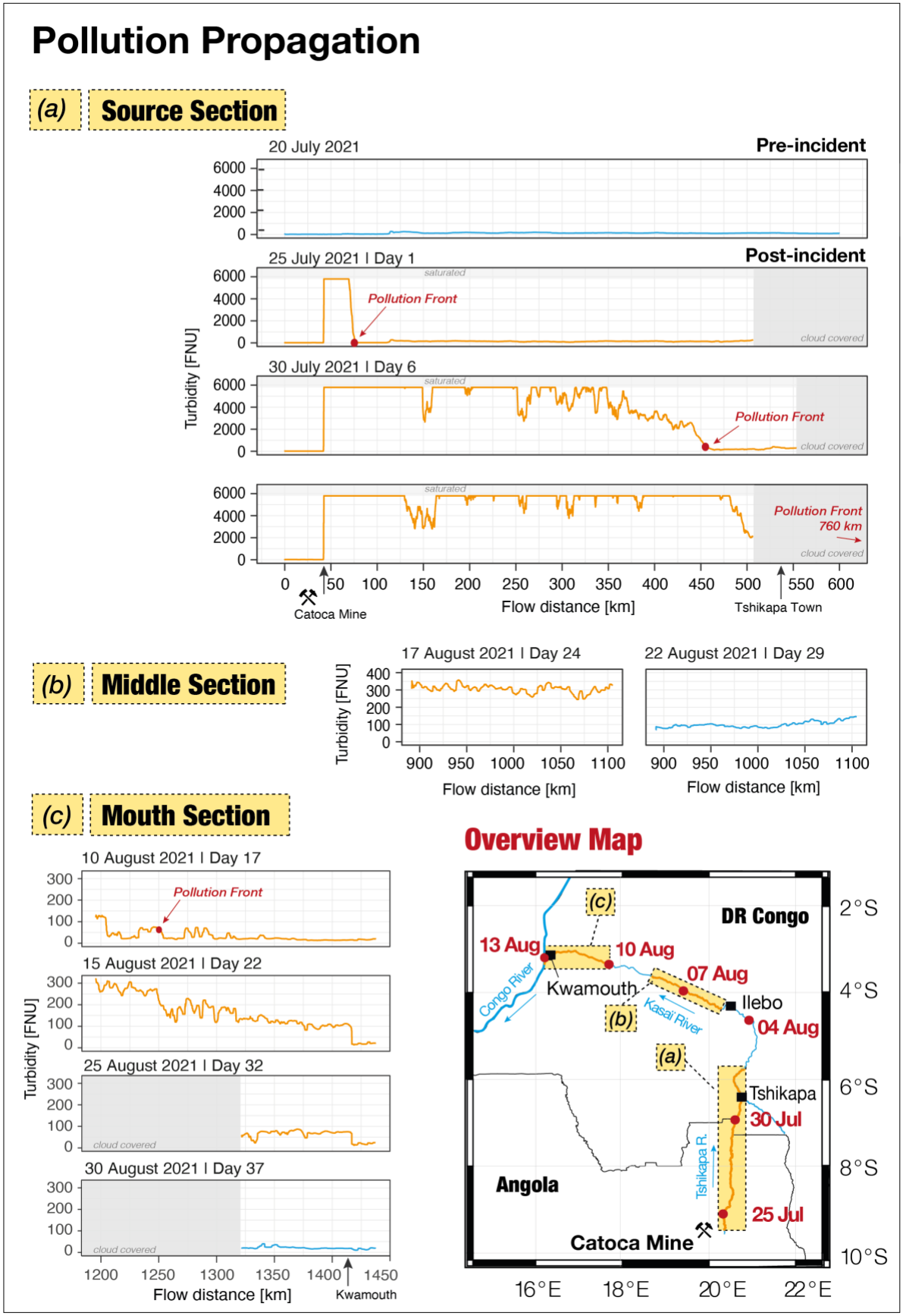

Figure 5 Comparison between pre- and post-incident turbidity [FNU] along the river flow [km]. Moving average over 300- pixel window for different sections of the river system. (a) Source section: first 600 km in Tshikapa River after the Catoca Mine, turbidity values are saturated ≥ 5800 FNU (b) Middle section and (c) mouth section show turbidity in Kasaï River for 860 to 1070 km and 1195 to 1440 km, respectively. (a), (b), (c) Blue color indicates background turbidity and orange color spill-affected turbidity when the pollution front has reached the river section. Scales differ

for y- axis. Overview map indicates the three river sections that were analyzed and red points the position of the pollution front for the respective dates based on visual identification on Sentinel-2 imagery.

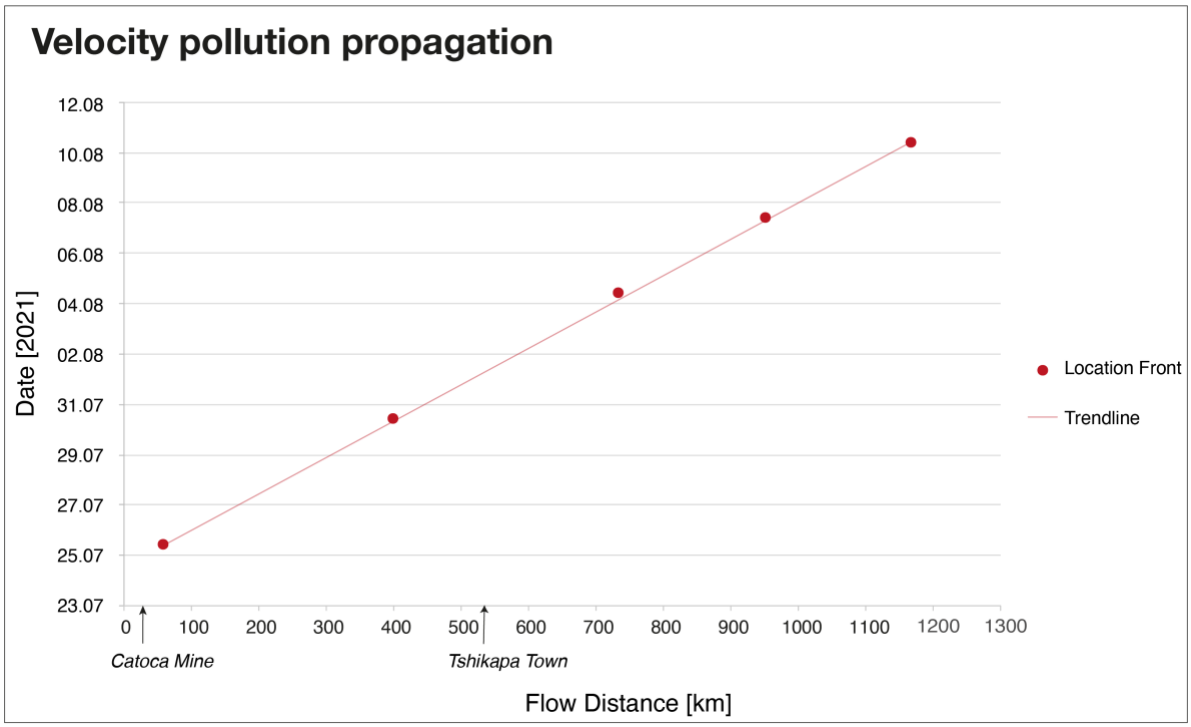

Figure 6 Plotting of location of pollution front (coordinates in Suppl.-Table 3) results in an almost linear (R^2= 0.9998) propagation speed with median and arithmetic mean of 0.81 m s^{-2}

4.2 Time series in Tshikapa River close to Catoca Mine

We defined a pair of virtual stations in the Tshikapa River, where one virtual station was located 5.24 km upstream of the inflow of Lova River and one 4.62 km downstream, respectively (coordinates in Suppl.-Table 1 in Appendix). For these virtual stations we extracted the turbidity from 382 Sentinel images sensed between October 2015 and December 2021. We calculated the median turbidity obtained from 3x3 pixel boxes in order to avoid mixed pixels. At these two virtual stations, mixed pixel artifacts are minimal and the time series are the most consistent across all locations we tested. Only three observations were affected by broken clouds, which we removed manually (dates in Suppl.-Table

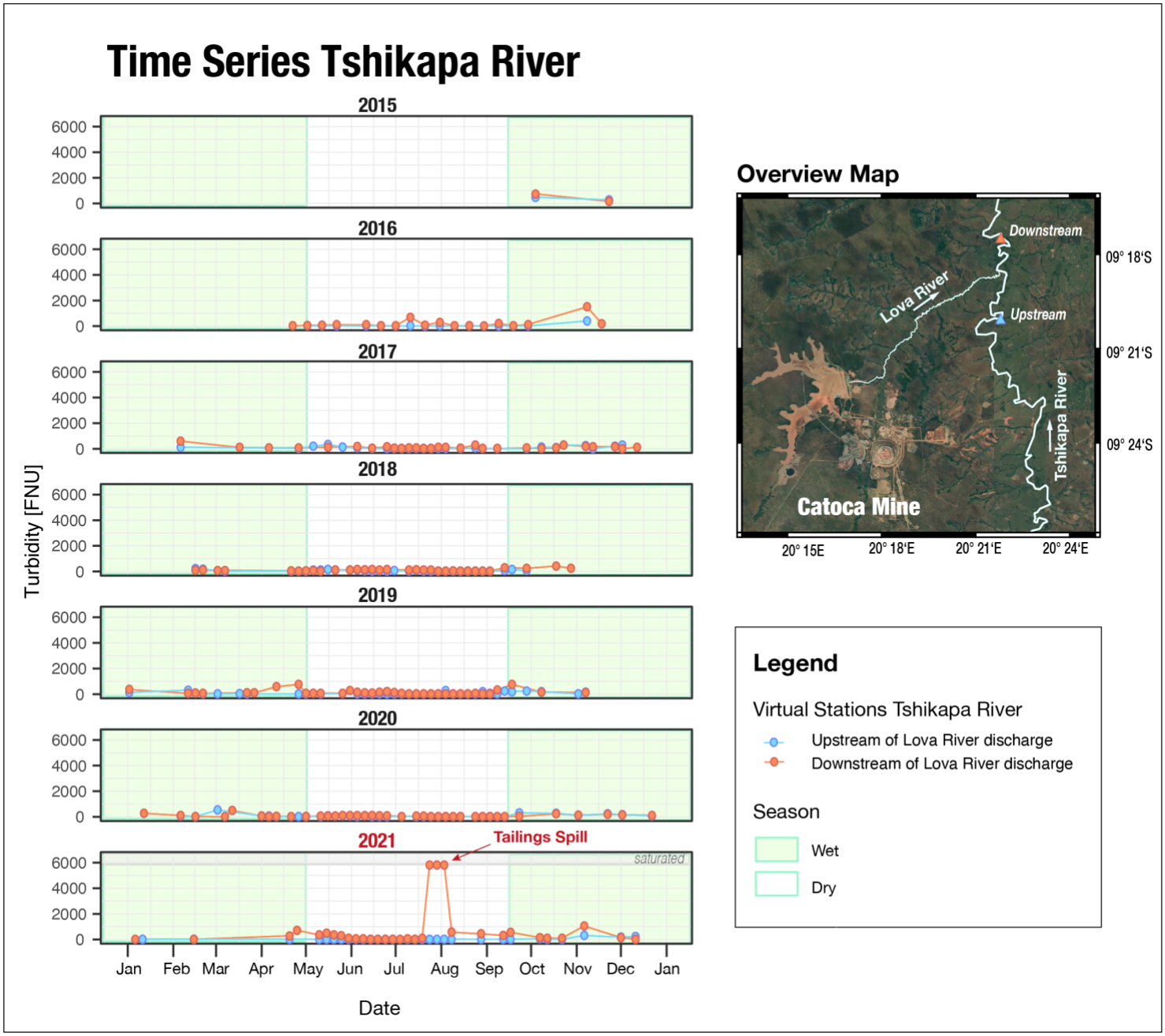

Figure 7 Turbidity from October 2015 to December 2021 for a pair of virtual stations in the Tshikapa River upstream and downstream of Lova River discharge, respectively. Dry- and wet season boundaries are only indicative, the exact onset of the rains varies from year to year. Overview Map: The Lova River which receives the spill-over of the mine and is a tightly meandering for 18.6 km North-East to join the Tshikapa River. Satellite Image of the Catoca Mine, Angola from Google Earth Pro 7.3.4.8248 (August 01, 2021). 09° 24' 15.15"S, 20° 18' 06.42"E, Eye alt 15.76 km. Maxar Technologies 2022. https://www.earth.google.com [March 14, 2022].

1 in Appendix). For the six-year-time series of these two stations, the median from the 3x3 window is available on 184 and 190 dates for the up- and downstream virtual station, respectively (Figure 7). Due to cloud coverage, pixel extraction was less successful during the wet season. Values are available at the upstream virtual stations for 114 dates in dry and 70 dates in the wet season and at downstream virtual stations for 112 dates in dry and 78 dates in the wet season, respectively.

In tropical regions, seasonality relates to increased sediment transport from soil erosion and mobilization of bedload during precipitation periods (Mushi et al., 2022). This is reflected by higher turbidity in the wet season than in the dry season at both virtual stations in the Tshikapa River from 2015 to 2020 (for summary statistics see Table 2). Visual inspection of the Sentinel-2 imagery confirms that the turbidity of the river water shows higher values from early October onward since the entire North -South stretch of Tshikapa River shows a brownish color.

Table 2 Turbidity [FNU] of the virtual station upstream-wide and downstream-wide with respect to the inflow of the Lova River respectively. Columns show values for the years 2015-2020 and 2015-2021.

	Upstream				**Downstream**			
	2015 – 2020		2015 – 2021		2015 – 2020		2015 – 2021	
	median	max	median	max	median	max	median	max
Dry Season	22	341	21	341	70	684	71	**5800**
Rainy Season	75	539	57	539	105	1503	112	1503

For 170 dates between 2015 and 2021, turbidity values are available for both stations. In over 80% of the cases, downstream values slightly to moderately exceeded upstream values (Histograms for dry and wet season in Suppl.-Figure 1 in Appendix). In a fifth of the cases, downstream turbidity was lower than upstream which suggest that the Lova River occasionally has a dilution effect on the turbidity in the Tshikapa River, mainly during the rainy season. The highest differences of turbidity between up- and downstream of the Lova inlet can be observed during the spill. On 20 July 2021 upstream turbidity was below 20 FNU while downstream turbidity approached 100 FNU reflecting a usual ratio for the dry season (Table 2). Five days later, on 25 July, turbidity values downstream suddenly jumped to the saturation value of 5800 FNU where they remain until 4 August 2021. These turbidity values represent the maximum of the entire time series and an at least 60-fold increase compared to prior to the spill. For the same time period, values at the virtual station upstream remained stable and below 20 FNU resulting in a difference of two orders of magnitude between upstream and downstream. On 9 August 2021 turbidity values downstream are still elevated, however a magnitude lower than five days earlier. Downstream values reach pre-incident levels only in early October after the onset of rainfall.

5 Discussion

5.1 Timing and extent of the Catoca tailings spill

The pixel extractions and the visual observations of the Sentinel-2 imagery confirm that the tailings spill occurred between 20 and 25 July 2021. Based on the calculated propagation velocity of the pollution front we date the incident to 24 July 2021. The mine management had initially stated that the incident happened on 27 July (Sociedade Mineira de Catoca Lda., 2021) but in an Angolan television broadcast of late September, another date, namely the 24 July 2021, was mentioned (Santos, 2021). Other researchers also dated the incident to the 24 July 2021 based on composite maps of 1-meter resolution imagery of commercial satellites (Petley, 2021).

The time series of the Tshikapa River at the level of the Catoca mine confirms that, in the 6 past years, there has never been turbidity values as high as the signal sensed from 25 July to 4 August 2021 following the tailings spill. The time-series suggests that the spilling of tailings was not totally stopped by end of July, as the company stated (Sociedade Mineira de Catoca Lda., 2021), but that a high sediment load was discharged into Lova River until mid-September 2021. Our pixel extraction along the river course allowed following the pollution signal from the starting point where the Lova River discharges the mine effluent into the Tshikapa River. The pollution front crossed the border into the Congolese Kasaï Province on 30 July 2021 and, according to our calculations, reached the town of Tshikapa on 31 July 2021. At Tshikapa town, the Tshikapa River discharges into the Kasaï River, a main tributary to the Congo River. Even after the confluence, the pollution signal did not dissipate but the Kasaï River carried the pollution front for another 880 km of flow distance to its confluence with the Congo River where it arrived 20 days later on 13 August 2021. At the mouth of the Kasaï River, the 30 August coincided with the first image where turbidity levels reached pre-incident levels. Thus, our methodology allowed following the pollution signal for over 1400 km and for 32 days, which has a great potential for documenting large-scale pollution incidents caused by failures at tailings storage facilities.

Although we also noticed the impacts of mining activities on turbidity levels prior to the incident, the drastic increase in turbidity after the tailings spill was unprecedented. The dataset showed that median turbidity levels of the pollution wave were several 10-fold higher than prior to the incident. The same large differences appear when comparing pixels along the Tshikapa river path before and after the incident. These observations clearly contradict statements of company representatives and government officials saying that turbidity levels were within usual ranges compared to those caused by other mining activities.

Elevated turbidity levels reflect a higher concentration of suspended particles in the water. Since less light penetrates a turbid water column, aquatic vegetation produces less oxygen through photosynthesis which affects aquatic biota (EPA, 2021). High turbidity has also direct lethal effects on fish by damaging and/or clogging fish gills and leading to asphyxiation (Bash et al., 2001). The mortality of fish depends not only on the concentration of suspended sediments, but also on its particle size, on the duration of exposure and the fish species and its life stage (Bash et al., 2001). Turbidity can be translated into total

suspended solids (TSS) concentration via a linear correlation (Eq. 4) (Rasmussen et al., 2009). A median turbidity of around 5800 FNU within the main pollution front translates to TSS concentrations of 4.9 g L^{-1}. This value exceeds the Angolan fresh water standard of 60 mg L^{-1} for TSS (República de Angola, 2011) and the Congolese value of 80 mg L^{-1} (Tshamala et al., 2021) by factors of 80 and 60, respectively. Even ten days after the pollution front arrived in the section between Ilebo and Bandundu, turbidity values remained close to 300 FNU, which translates into 300 mg L^{-1} and is still about 4-fold higher than Congolese fresh water reference standards. This means that it is very likely that the spill caused health impacts on individuals who consumed water of the Tshikapa- and Kasaï Rivers between 31 July and 17 August 2021.

These suspended sediment concentrations were also close to 50-fold above the threshold value of 100 mg L^{-1} for healthy fish populations and other aquatic biota in streams (Chapman et al., 2017). Since turbidity remained as high for over 10 days, we must conclude that the tailings spill caused lethal impacts on fish populations in Tshikapa River and Kasaï River as it was reported by the riparian population. Not only is acute mortality of such pollution incidents of concern for aquatic biota, but the particles released during the tailings spill can harm ecosystem for longer time. Particles can clog the stream bed which impacts the breeding sites of fish and benthic macroinvertebrates (EPA, 2021). Also, high flow rates will re-suspend deposited tailings: For the months after the Feijao dam failure in Brumadinho, Brazil, a study demonstrated that a large volume of tailing deposits in the Paraopeba River was resuspended during the rainy season (Teixeira et al., 2021).

Optical remote sensing cannot provide data on metal concentrations, but authors used total suspended solids (TSS) and turbidity as proxies for evaluation of metal transport in river water (Nasrabadi et al., 2016; Swain and Sahoo, 2017). Chemical analyses of mining effluents showed that heavy metals were mostly bound to suspended particles such as iron- and manganese oxyhydroxides and other colloids and that heavy-metal transport was more significant in the suspended than in the dissolved form (Kimball et al., 1995; Telmer and Stapper, 2007; Cánovas et al., 2008; Sracek et al., 2012). Numerous studies revealed a high pollution potential of tailings since the small- sized particles may release high concentrations of toxic metals and acids (Kříbek et al., 2010; Mudd and Boger, 2013; Roca et al., 2019). It is well documented, that diamond mines in Canada, Russia, South Africa with the same ore type as Catoca, exhibit pollution risks with regard to mine waste due to the release of toxic metals such as cadmium, copper, lead, molybdenum, nickel and mercury (Strydom, 2015; Independent Environmental Monitoring Agency, 2019; Legostaeva and Gololobova, 2021). Therefore, it is misleading when the mine operators describe tailings as a "*mixture of natural rocks... that does not represent a risk of life for the affected populations*" (Sociedade Mineira de Catoca Lda., 2021).

For the Catoca spill, the debate on the consequences and the severity of the incidents are still ongoing with the company downplaying the social and environmental impacts and refusing to acknowledge that the spill had any toxic effects (Santos, 2021; TPA, 2021c; VoA Português, 2021b). Since September, no official statements were released, neither by the Congolese, nor by the Angolan government. Neither fishermen nor riparian communities received any compensation for negative health impacts or economic losses to date. However, a trial was initiated on 21 March 2022 against the Sociedade Mineira de Catoca Lda. at the High Court of Tshikapa to seek reparation (Muamba, 2022).

5.2 Transfer of the methodology to other tailings dam incidents

In this section, we discuss the applicability of the new methodology to a number of major tailings dam incidents that occurred since the launch of the first Sentinel-2 satellite in June 2015. In recent years, the Sentinel-2 mission became popular for monitoring inland water bodies (Sheffield et al., 2018; Nouchi et al., 2019) and rivers (Warren et al., 2019; Li et al., 2020a; Lu et al., 2020; Wang et al., 2021). Its main advantages are the relatively high resolution of 10 to 20 meters in the visible and near-infrared spectrum, the fast revisit times of five days at the Equator and only 2-3 days at higher latitudes. For comparison, NASA's Landsat 8 (NASA, 2021) satellite mission has only 30 meters resolution in the visible spectrum preventing the analysis of small streams. The slow repeat-cycle of 16 days at the equator also hampers adequate tracking of a water pollution incident with Landsat 8. Restricted access missions such as the Pléiades (1A and 1B) and the SPOT satellites (6 and 7) from the French government space agency CNES were launched a few years earlier than Sentinel-2 and impress with their high spatial resolution of 0.5 m and 1.5 m, respectively, for three visible- and one infrared bands. However, high purchasing costs, inconsistent revisit times and irregular imagery footprints for locations around the globe make these satellites unsuitable for monitoring pollution incidents. Similarly, Planet Labs Inc.'s fleet of over 180 miniaturized and light-weight 'nanosatellites' from the Dove mission and its 5 Rapid Eye satellites offer no valid alternative to Sentinel-2. Not only the small swath of the imagery and irregular revisit times, but foremost the low radiometric quality of the cheaper nanosatellite sensors preclude water quality monitoring (Nagel et al., 2020).

To discuss the potential of transferring the methodology to other tailings dam incidents we made use of the continuously updated online database on tailings dam failures from the WISE Uranium Project (WISE Uranium Project, 2022). The list comprises dam failures or tailings spills at active mine sites and at abandoned workings and includes spills at (aluminum) processing plants and collapses of mine waste heaps that triggered landslides. The reported volume of mobilized tailings is often unknown but ranges from less than 10'000 m^3 to over 30 Mio m^3. The database also contains a qualitative description of the environmental impacts of the tailings spill such as the travel distance of a spill along a river system. For our analysis, we filtered the 26 incidents recorded between the start of the Sentinel-2 mission in June 2015 and August 2021. We classified the incidents based on a simple decision tree: We first selected incidents that occurred at tailings storage facilities in mining areas and that mobilized tailings volumes of at least > 50'000 m^3 and/or where tailings had reportedly affected surface water bodies. For the incidents that fulfill these requirements, we checked the availability of Sentinel-2 data and verified the cloud coverage of each image (Table 3).

The review of the incidents demonstrated that the doubling of Sentinel-2 data availability with the launch of Sentinel-2B in 2017 has significantly improved the mission's capability to monitor mining incidents. Between 2015 and 2017, the mission relied only on Sentinel-2A, and had therefore revisit times of 10 days at the equator. In addition, only little imagery outside of Europe is available from the first year after launch.

Table 3 Categorization of 26 tailings dam incidents that were reported after June 2015 by WISE uranium project. Black dots (●) if condition applies, crosses (x) if condition doesn't apply or (N/A) if information is not available or the condition not applicable. Category of cloud coverage only assessed for S-2 imagery that covers incident. Orange background for incidents with a high potential for analysis with the methodology presented in this paper.

Sentinel-2 satellites	Date of incident	Location	Decision tree			Imagery	
			Mine Site	*Volume released > 50'000 m^3*	*Tailings mobilized in rivers*	*S-2 covers incident*	*Low cloud coverage*
A	2015-11-05	Germano mine, Bento Rodrigues, distrito de Mariana, Região Central, Minas Gerais, Brazil	●	●	x	x	N/A
A	2015-11-21	San Kat Kuu, Hpakant, Kachin state, Myanmar	●	●	x	x	N/A
A	2015-12-14	Lamaungkone, Hpakant, Kachin state, Myanmar	●	●	N/A	x	N/A
A	2016-05-22	Ridder, Kazakhstan	●	●	N/A	x	N/A
A	2016-08-04	Ujina, Pica, Tamarugal Province, Tarapacá Region, Chile	●	x	N/A	x	N/A
A	2016-08-08	Dahegou Village, Luoyang, Henan province, China	x	N/A	N/A	x	N/A
A	2016-08-27	New Wales plant, Mulberry, Polk County, Florida, USA	x	x	x	x	N/A
A	2016-10-27	Antamok mine (inactive), Itogon, Benguet province, Philippines	●	●	●	x	N/A
A	2016-12-28	Satemu, Hpakant, Kachin state, Myanmar	●	●	N/A	x	N/A
A	2017-03-12	Tonglvshan Mine, Hubei province, China	●	●	x	x	N/A
A	2017-06-30	Mishor Rotem, Israel	●	x	x	N/A	N/A
A&B	2017-09-17	Kokoya Gold Mine, Bong County, Liberia	●	x	N/A	N/A	N/A
A&B	2018-02-17	Barcarena, Pará, Brazil	x	●	●	N/A	N/A
A&B	2018-03-03	Huancapatí, Recuay province, Áncash region, Peru	●	●	●	●	x
A&B	2018-03-09	Cadia, New South Wales, Australia	●	x	x	N/A	N/A
A&B	2018-06-04	Cieneguita mine, Urique, Chihuahua, Mexico	●	●	●	●	●
A&B	2019-01-25	Córrego de Feijão mine, Brumadinho, Minas Gerais, Brazil	●	●	●	●	x
A&B	2019-03-29	Machadinho d'Oeste (inactive), Oriente Novo, Rondônia, Brazil	●	x	x	N/A	N/A
A&B	2019-04-09	Muri, Jharkhand, India	x	N/A	x	N/A	N/A
A&B	2019-04-22	Hpakant, Kachin state, Myanmar	●	●	N/A	●	●
A&B	2019-07-10	Cobriza mine, San Pedro de Coris district, Churcampa province, Huancavelica region, Peru	●	●	●	●	●
A&B	2019-10-01	Nossa Senhora do Livramento, Mato Grosso, Brazil	●	x	x	N/A	N/A

Sentinel-2 satellites	Date of incident	Location	Decision tree			Imagery	
			Mine Site	*Volume released > 50'000 m³*	*Tailings mobilized in rivers*	*S-2 covers incident*	*Low cloud coverage*
A&B	2020-03-28	Luming Mine, Tieli, Yichun City, Heilongjiang Province, China	●	●	●	●	●
A&B	2020-05-01	San José de Los Manzanos, Canelas, Durango, Mexico	●	x	N/A	N/A	N/A
A&B	2020-07-02	Hpakant, Kachin state, Myanmar	●	●	●	●	x
A&B	2021-07-27	Catoca mine, Saurimo, Lunda Sul, Angola	●	●	●	●	●

We will briefly discuss three incidents from Table 3 to illustrate this limitation. For the Fundão tailings dam at the Germano mine that failed on 5 November 2015, there is no Sentinel-2 imagery available to cover the incident. Only three weeks after the incident, a first Sentinel-2 image (with high cloud cover) covers the area of interest. Authors that studied this devastating incident mapped surface water turbidity at the mouth of Doce River in the Atlantic Ocean based on lower resolution Landsat TM 5 and Landsat 8 OLI images (Rudorff et al., 2018). For another tailings dam failure at the Antamok mine in the Philippines on 27 October 2016 that reportedly polluted the river system, a Sentinel-2 image of the tile where the mine is located exists close to the incident date, but due to cropping it fails to reveal the area of interest. A third notable example of an incident that falls into the beginning of the Sentinel- 2 mission is the tailings dam failure at Glencore's Kazzinc Mine in Ridder, Kazakhstan, that occurred on 22 May 2016. The release of nearly 400 000 m^3 of tailings polluted the Filippovka-, the Ulba- and the Irtysh Rivers and allegedly threatened the residents of the metropolitan region of Omsk in neighboring Russia some 1100 km away (Ivanshenko, 2016; Kaparov, 2016; Malikov, 2016; The Siberian Times Reporter, 2016). For this incident, barely any Sentinel-2 imagery exists. For the mine location and surrounding areas until the city of Semey, there is some (cloudy) imagery available prior to the incident, but no other image was sensed during the rest of May 2016. The first post-incident image of the mine and surrounding areas is from early June 2016.

From these observations, we can conclude that Sentinel-2 imagery is only useful for tracking pollution incidents after the mission was fully operational some months after the launch of the second satellite on 07 March 2017. This reduces the initial list of 26 incidents to 15 cases (Table 3). The applicability of our method is not only limited by availability of imagery but also by data quality. Cloud coverage, a known limitation of optical remote sensing, poses a significant limitation to the analysis of many incidents. Not only dense cirrus clouds block the surface reflectance from reaching the satellite sensor but also haze and thin clouds can cause interferences and affect surface reflectance (Pahlevan et al., 2022). This is particularly relevant for tailings dam failures since about 40% of incidents in post-2000 were at least partly triggered by heavy rainfall events (Azam and Li, 2010). Especially in tropical regions with pronounced wet seasons, dense cloud coverage lasts for several weeks to months. This is particularly relevant for areas with monsoon-driven climate such as the Jade producing mines of the Hpakant region in Myanmar, where almost every year a recorded incident was related to precipitations events (Table 3). The steep slopes of the mine waste piles collapsed and triggered flood waves in adjacent pit lakes that buried numerous workers (WISE Uranium Project, 2022). The deadliest event

occurred on 2 July 2020 and left more than 175 people dead (WISE Uranium Project, 2022). However, for the Hpakant region, no cloud-free images are available between mid-May and October 2020. Only one incident in Hpakant occurred before the wet season in April 2019 and could potentially be evaluated with the presented methodology.

Climatic conditions also limit the potential to track tailings dam incidents in other mining regions in the world. Among the intensively mined areas in Latin America, the southern extent of the 5000 km long Andes Cordillera is known for intense precipitation and high cloud coverage (Barrett et al., 2009). A case in point is the dam failure of the Huancapati mine in Chile on 03 March 2018, for which no acceptable imagery exists. In addition, the devastating incident of the Brumadhino tailings dam in Brazil of 25 January 2019 disappeared under dense clouds for more than a month after the incident.

In addition to the Hpakant incident, we identified three other tailings dam failures that have a potential be studied using our Sentinel-2 workflow (Table 3). 1) the Cobriza copper mine in Huancavelica region, Peru (10 July 2019), 2) the Cieneguita gold and silver mine in Chihuahua, Mexico (04 June 2018) and 3) the Luming molybdenum mine in Heilongjiang Province, China (28 March 2020). We recommend analyzing water quality impacts of those four tailings spill incidents with the Sentinel-2 workflow presented in this study.

Overall, the Catoca tailings incident was a highly suitable case for pollution tracking regarding the availability and the quality of Sentinel-2 multi-spectral imagery to cover the first few hundreds of kilometers along the river system. First, the incident happened at the end of the dry season where cloud coverage generally was low. In the weeks that followed the spill, the climate transited to the rainy season and cloud coverage increased. Especially in the North of our region of interest closer to the Equator, there was a lot of haze on the imagery. Further, the pollution propagated in river system, which was oriented mainly in a South to North direction for over 780 km, from the Catoca mine to the town of Ilebo. This perfectly suited the path of the polar-orbiting Sentinel-2 satellites, which means that, for each sensing day, a coherent compilation of juxtaposed tiles in North- South direction was available which significantly reduces the workload for image mosaicking. The continuity in image coverage for the same day becomes trickier if the pollution would rather propagate in longitudinal direction. We observed this additional challenge when monitoring the flow of the river in East to West direction between the city of Ilebo and Kwamouth, the mouth of the Kasaï River reaching the Congo River. For the last 620 km of flow distance, we had to switch MSI swaths twice which comes with a considerable effort of mosaicking and the difficulty in plotting the data chronologically.

6 Conclusion

Strong global economic growth continues to stimulate the demand for manufactured goods and fossil energy carriers and therefore thrives the extraction of mineral resources in an unprecedented pace (Reichl et al., 2020). The tendency to extract lower and lower ore grades leads to an ever-increasing amount of ore processing waste that is deposited every year within over 18 000 dammed tailing storage facilities (TFS) around the world, of which 0.12 ‰ fail (Azam and Li, 2010). Large amounts of tailings are released with devastating consequences on the environment and human health (Cheng et al., 2021;

Rana et al., 2021). Water bodies are affected the most, but human and financial capacities in producer countries are often inadequate for assessing the large-scale impacts and incidents remain highly debated. Here, we demonstrated how remote sensing supports the assessment of large-scale water quality impacts of tailings spills and adds to the evidence base in data-scarce regions where riparian communities still wait for the recognition and the compensation of damage. We presented a satellite remote sensing workflow to analyze the magnitude and the extent of a pollution incident where tailings polluted a large river system.

We applied this new workflow to the controversial tailings spill at the Catoca diamond mine in Angola, that caused a diplomatic incident between Angola and DR Congo following accusations of fatalities as a consequence of the pollution. We used high-resolution satellite imagery of ESA's Sentinel-2 mission to extract turbidity as a water quality parameter for the river system. Although, the tailings spill at the Catoca mine had left only minor land-cover changes in the Lunda Sul Province in Angola, our data illustrates that the incident had major and far-reaching impacts with regard to water quality. We were able to clear controversies about timing of the incident, dating it to midday of 24 July 2021. A 6- years-time series of the turbidity at the level of the mine showed that the values exceeded anything previously measured. Turbidity values increased up to several orders of magnitude, which evidenced that the impacts of the spill were severe. We were able to track the pollution signal downstream from Angola into the DR Congo for over 1400 km until it reached the Congo River 20 days after the spill had started. The high turbidity values left no doubt that this tailings spill caused large fish kills. It is highly probable that human beings who consumed the river water in Lunda Norte Province, Angola between 25 July and 10 August and in the Kasaï Province, DR Congo between 30 July and 17 August suffered severe health effects.

In addition to our in-depth analysis of the Catoca spill we studied the feasibility of applying the methodology to other tailings dam failures that occurred since the start of the Sentinel-2 mission. We illustrated the data limitations before the Sentinel-2 mission was fully operational in 2017, problems caused by cloud cover but also opportunities to apply our workflow to learn more about the dynamics and extend of tailings dam failures. Finally, we identified four tailings-related pollution incidents in Peru, Mexico, China and Myanmar, where the new workflow could be used for assessing water quality impacts.

Data availability statement

The code and imagery supporting the conclusions of this article are available under the following link: https://github.com/JamesRunnalls/catoca-tailings-failure

Author contributions

DR designed and implemented the study under the guidance of DO. JR programmed the river skeletonizing algorithm and DO and JR performed the atmospheric correction of the satellite imagery and the pixel extraction. DR analyzed and interpreted the dataset and wrote the manuscript. RT was

involved in the conception of the study. BW has provided support to orient the study and to edit the manuscript. All authors discussed the results and commented on the manuscript.

Acknowledgment

We thank Stany Frank for providing photographs of the Kasaï River after the pollution incident. Heresh Fattahi from Jet Propulsion Laboratory at Caltech is acknowledged for the discussions about satellite technologies. Francesco Wyss from Swisstopo National Point of Contact provided information on commercial satellite imagery. We thank Rosi Siber for compiling the hydrologic map of the study area.

References

Alrosa (2021). Sociedade Mineira de Catoca, Limitada (CATOCA, Limitada). Available at: http://eng.alrosa.ru/corporate-structure/sociedade-mineira-de-catoca-catoca-ltd/ [Accessed November 22, 2021].

AMDC (2017). Report on artisanal and small-scale mining in Africa . Selected Countries Policy Profile Review on ASM. African Minerls Development Centre, United Nations Economic Commission for Africa.

Azam, S., and Li, Q. (2010). Tailings dam failures: A review of the last one hundred years. *Geotech. News* 28, 50–53.

Barrett, B. S., Garreaud, R. D., and Falvey, M. (2009). Effect of the Andes Cordillera on Precipitation from a Midlatitude Cold Front. *Mon. Weather Rev.* 137, 3092–3110. doi:10.1175/2009MWR2881.1.

Bash, J., Berman, C., and Bolton, S. (2001). Effects of Turbidity and Suspended Solids on Salmonids. *Measurement*, 74.

BFG (2022). Global Runoff Data Centre. Available at: https://www.bafg.de/GRDC/EN/02_srvcs/21_tmsrs/riverdischarge_node.html [Accessed March 22, 2022].

Byrne, P., Hudson-Edwards, K. A., Bird, G., Macklin, M. G., Brewer, P. A., Williams, R. D., et al. (2018). Water quality impacts and river system recovery following the 2014 Mount Polley mine tailings dam spill, British Columbia, Canada. *Appl. Geochemistry* 91, 64–74. doi:10.1016/j.apgeochem.2018.01.012.

Cánovas, C. R., Hubbard, C. G., Olías, M., Nieto, J. M., Black, S., and Coleman, M. L. (2008). Hydrochemical variations and contaminant load in the Río Tinto (Spain) during flood events. *J. Hydrol.* 350, 25–40.

Cavalheiro Paulelli, A. C., Cesila, C. A., Devóz, P. P., Ruella de Oliveira, S., Bianchi Ximenez, J. P., Pedreira Filho, W. dos R., et al. (2022). Fundão tailings dam failure in Brazil: Evidence of a population exposed to high levels of Al, As, Hg, and Ni after a human biomonitoring study. *Environ. Res.* 205, 112524. doi:10.1016/j.envres.2021.112524.

Chapman, P. M., Hayward, A., and Faithful, J. (2017). Total Suspended Solids Effects on Freshwater Lake Biota Other than Fish. *Bull. Environ. Contam. Toxicol.* 99, 423–427. doi:10.1007/s00128-017-2154-y.

Cheng, D., Cui, Y., Li, Z., and Iqbal, J. (2021). Watch out for the tailings pond, a sharp edge hanging over our heads: Lessons learned and perceptions from the brumadinho tailings dam failure disaster. *Remote Sens.* 13. doi:10.3390/rs13091775.

Clarkson, L., and Williams, D. (2021). An Overview of Conventional Tailings Dam Geotechnical Failure Mechanisms. *Mining, Metall. Explor.* 38, 1305–1328. doi:10.1007/s42461-021-00381-3.

COBA Group (2015). Angola - Aproveitamento Hidroeléctrico de Chicapa II, na Lunda Sul. Available at: http://www.cobagroup.com/NOTICIAS/arq_2015/arquivo_2015_PT.html [Accessed January 19, 2022].

CRREBac (2021). Pollution des rivières Tshikapa et Kasaï identifiée dans l'Outil CB -CIS : Appel à l'action du CRREBaC. Kinshasa: Centre de recherche en Ressources en Eau du Bassin du Congo.

Cumena, J. T. D., Neto, José Alves, F., Carvalho, A. E. S., and Souza, P. A. F. de (2019). Estudos no âmbito do setor de extração de diamantes em Angola e seus impactos socioeconômicos. *Rev. Bras. Geogr. Física* 12, 121–1230.

Da Cruz, Y. da C. C. (2016). Estudos geotécnicos de uma barragem de aterro em Angola – Fase de concurso.

da Silva Souza, T., da Silva Figueira Barone, L., Lacerda, D., dos Santos Vergilio, C., de Oliveira, B. C. V., de Almeida, M. G., et al. (2021). Cytogenotoxicity of the water and sediment of the Paraopeba River immediately after the iron ore mining dam disaster (Brumadinho, Minas Gerais, Brazil). *Sci. Total Environ.* 775, 145193. doi:10.1016/j.scitotenv.2021.145193.

de Lucia Lobo, F., Costa, M., De Moraes Novo, E. M. L., and Telmer, K. (2017). Effects of small-scale gold mining tailings on the underwater light field in the Tapajós River Basin, Brazilian Amazon. *Remote Sens.* 9. doi:10.3390/rs9080861.

Dijkstra, E. W. (1959). A note on two problems in connexion with graphs. *Numer. Math.* 1, 269–271.

Dogliotti, A. I., Ruddick, K. G., Nechad, B., Doxaran, D., and Knaeps, E. (2015). A single algorithm to retrieve turbidity from remotely-sensed data in all coastal and estuarine waters. *Remote Sens. Environ.* 156, 157–168. doi:10.1016/j.rse.2014.09.020.

EPA (2021). Water Monitoring and Assessment. 5.5. Turbidity. Available at: https://archive.epa.gov/water/archive/web/html/vms55.html [Accessed February 15, 2022].

ESA (2015). Sentinel-2 User Hand. Paris: European Space Agency doi:10.1021/ie51400a018.

ESA (2021). Sentinel-2. Available at: https://sentinel.esa.int/web/sentinel/missions/sentinel-2 [Accessed November 22, 2021].

Frazão, R., Catarino, S., Goyder, D., Darbyshire, I., Magalhães, M. F., and Romeiras, M. M. (2020). Species richness and distribution of the largest plant radiation of Angola: Euphorbia (Euphorbiaceae). *Biodivers. Conserv.* 29, 187–206. doi:10.1007/s10531-019-01878-6.

Freitas, C. M., and Da Silva, M. A. (2019). Work accidents which become disasters: Mine tailing dam failures in Brazil. *Rev. Bras. Med. do Trab.* 17, 21–29. doi:10.5327/Z1679443520190405.

Ghahramani, N., Mitchell, A., Rana, N., McDougall, S., Evans, S., and Take, A. (2020). Tailings-flow runout analysis: Examining the applicability of a semi-physical area–volume relationship using a novel database. *Nat. Hazards Earth Syst. Sci.*, 1–23. doi:10.5194/nhess-2020-199.

Global Witness (2015). Myanmar's "Big State Secret": The Biggest Natural Resources Heist in Modern History?

Google LLC. (2021). Google Earth Pro.

Guo, F., Wu, F. C., Yu, F., Bai, Y. C., Fu, Z. Y., Zhu, Y. R., et al. (2019). Fate and removal of antimony in response to stringent control activities after a mine tailing spill. *Sci. Total Environ.* 693. doi:10.1016/j.scitotenv.2019.133604.

Gupta, R., and Shankar, H. (2022). Global Energy Observatory - Chicapa-1 Dam Hydroelectric Power Plant. Available at: http://globalenergyobservatory.org/geoid/2658 [Accessed March 28, 2022].

Hijmans, R., Rojas, E., Cruz, M., O'Brien, R., and Barrantes, I. (2018). DIVA-GIS. *Ctry. Lev. data*. Available at: http://www.diva-gis.org/Data [Accessed October 10, 2020].

Holland, H., and Reid, H. (2021). Congo says Angola tailings pollution kills 12, to seek compensation.

Hudson-Edwards, K. A., Byrne, P., Bird, G., Brewer, P. A., Burke, I. T., Jamieson, H. E., et al. (2019). Origin and Fate of Vanadium in the Hazeltine Creek Catchment following the 2014 Mount Polley Mine Tailings Spill in British Columbia, Canada. *Environ. Sci. Technol.* 53, 4088–4098. doi:10.1021/acs.est.8b06391.

Huntley, B. J., Russo, V., Lages, F., and Ferrand, N. eds. (2019). *Biodiversity of Angola: Science and Conservation: A Modern Synthesis*. Cham, Switzerland: Springer Nature Switzerland AG doi:10.1007/978-3-030-03083-4_11.

Independent Environmental Monitoring Agency (2019). 2018-2019 Annual Report. Technical Language. Yellowknife, Canada.

Islam, K., and Murakami, S. (2021). Global-scale impact analysis of mine tailings dam failures: 1915–2020. *Glob. Environ. Chang.* 70, 102361. doi:10.1016/j.gloenvcha.2021.102361.

Ivanshenko, N. (2016). Утечка стоков с завода «Казцинк» в ВКО ликвидирована.

Kaparov, E. (2016). Урон, причиненный «Казцинком» в ходе аварии в Риддере оценен в 4 млрд. *Environ. News*.

Kimball, B. A., Callender, E., and Axtmann, E. V. (1995). Effects of colloids on metal transport in a river receiving acid mine drainage, upper Arkansas River, Colorado, U.S.A. *Appl. Geochemistry* 10, 285–306. doi:10.1016/0883-2927(95)00011-8.

Köppen, W. (1936). *Das geographische System der Klimate*. , eds. W. Köppen and R. Geiger Berlin: Gebrueder Borntraeger doi:10.2307/200498.

Kraus, U., and Wiegand, J. (2006). Long-term effects of the Aznalcóllar mine spill-heavy metal content and mobility in soils and sediments of the Guadiamar river valley (SW Spain). *Sci. Total Environ.* 367, 855–871. doi:10.1016/j.scitotenv.2005.12.027.

Kříbek, B., Majer, V., Veselovský, F., and Nyambe, I. (2010). Discrimination of lithogenic and anthropogenic sources of metals and sulphur in soils of the central-northern part of the Zambian Copperbelt Mining District: A topsoil vs. subsurface soil concept. *J. Geochemical Explor.* 104, 69–86. doi:https://doi.org/10.1016/j.gexplo.2009.12.005.

Legostaeva, Y. B., and Gololobova, A. G. (2021). Long-term geochemical monitoring of the soil cover in the impact zone of diamond mining enterprises: a case study in the Nakyn kimberlite field, Russia. *Environ. Monit. Assess.* 193, 1–13. doi:10.1007/s10661-021-09087-x.

Lepoudre, C. (2018). Tailings Failure Case Studies, Statistics and Failure Modes Webinar.

Li, D., Wu, B., Chen, B., Qin, C., Wang, Y., Zhang, Y., et al. (2020a). Open-surface river extraction based on sentinel-2 MSI imagery and DEM Data: Case study of the upper yellow river. *Remote Sens.* 12. doi:10.3390/RS12172737.

Li, Q., Chen, Z., Zhang, B., Li, B., Lu, K., Lu, L., et al. (2020b). Detection of tailings dams using high-resolution satellite imagery and a single shot multibox detector in the Jing-Jin-Ji Region, China.

Remote Sens. 12. doi:10.3390/RS12162626.

Lu, X., Yang, K., Lu, Y., Gleason, C. J., Smith, L. C., and Li, M. (2020). Small Arctic rivers mapped from Sentinel-2 satellite imagery and ArcticDEM. *J. Hydrol.* 584, 124689. doi:10.1016/j.jhydrol.2020.124689.

Malikov, A. (2016). В Омск из Казахстана по реке плывут опасные химикаты.

Mendelsohn, J., Jarivs, A., and Robertson, T. (2013). A profile and atlas of the Cuvelai-Etosha basin. RAISON & Gondwana Collection.

Mining Technology (2021). Catoca Diamond Mine. Available at: https://www.mining-technology.com/projects/catoca-diamond-mine/ [Accessed November 22, 2021].

Moraga, J., and Gurkan, G. (2020). Monitoring The Impacts of a Tailings Dam Failure Using Satellite Images. 1–12.

Muamba, D. (2022). RDC – Justice : Début ce lundi 21 mars du procès opposant la société CATOCA d'Angola contre les victimes de la pollution des rivières Kasaï et Tshikapa.

Mudd, G. M., and Boger, D. V. (2013). The ever growing case for paste and thickened tailings - Towards more sustainable mine waste management. *AusIMM Bull.*, 56–59.

Munzimi, Y. A. (2019). Characterizing Hydrological Processes within the data-scarce environment of the congo basin.

Mushi, C. A., Ndomba, P. M., Tshimanga, R. M., Trigg, M. A., Neal, J., Bola, G. B., et al. (2022). Site Selection, Design, and Implementation of a Sediment Sampling Program on the Kasai River, a Major Tributary of the Congo River. 427–446. doi:10.1002/9781119657002.ch22.

Nagel, G. W., Márcia, E., Moraes, L. De, and Kampel, M. (2020). Nanosatellites applied to optical Earth observation : a review. doi:10.4136/1980-993X.

NASA (2021). Landsat 8.

Nasrabadi, T., Ruegner, H., Sirdari, Z. Z., Schwientek, M., and Grathwohl, P. (2016). Using total suspended solids (TSS) and turbidity as proxies for evaluation of metal transport in river water. *Appl. Geochemistry* 68, 1–9. doi:https://doi.org/10.1016/j.apgeochem.2016.03.003.

Natural Earth (2022). Natural Earth Data. Free verctor and raster map data. Available at: https://www.naturalearthdata.com/ [Accessed March 22, 2022].

Nechad, B., Ruddick, K. G., and Neukermans, G. (2009). Calibration and validation of a generic multisensor algorithm for mapping of turbidity in coastal waters. *Remote Sens. Ocean. Sea Ice, Large Water Reg. 2009* 7473, 74730H. doi:10.1117/12.830700.

Neto, G., and Maclean, R. (2021). Waste From Mine in Angola Kills 12 Downstream in Congo, Minister Says.

NetworkX (2022). singe_source_dijkstra. Available at: https://networkx.org/documentation/stable/reference/algorithms/generated/networkx.algorithms.shortest_paths.weighted.single_source_dijkstra.html [Accessed March 21, 2021].

Nouchi, V., Kutser, T., Wüest, A., Müller, B., Odermatt, D., Baracchini, T., et al. (2019). Resolving biogeochemical processes in lakes using remote sensing. *Aquat. Sci.* 81, 1–13. doi:10.1007/s00027-019-0626-3.

Odermatt, D., Gitelson, A., Brando, V. E., and Schaepman, M. (2012). Review of constituent retrieval in optically deep and complex waters from satellite imagery. *Remote Sens. Environ.* 118, 116–126. doi:10.1016/j.rse.2011.11.013.

Olías, M., Cánovas, C. R., and Basallote, M. D. (2021). Surface and Groundwater Quality Evolution in

the Agrio and Guadiamar Rivers After the Aznalcóllar Mine Spill (SW Spain): Lessons Learned. *Mine Water Environ.* 40, 235–249. doi:10.1007/s10230-020-00713-7.

Owen, J. R., Kemp, D., Lèbre, Svobodova, K., and Pérez Murillo, G. (2020). Catastrophic tailings dam failures and disaster risk disclosure. *Int. J. Disaster Risk Reduct.* 42. doi:10.1016/j.ijdrr.2019.101361.

PAC (2004). Revista anual da indústria dos diamantes. República de Angola 2004. Partnership Africa Canada (PAC).

Pahlevan, N., Mangin, A., Balasubramanian, S. V., Smith, B., Alikas, K., Arai, K., et al. (2021). ACIX-Aqua: A global assessment of atmospheric correction methods for Landsat-8 and Sentinel-2 over lakes, rivers, and coastal waters. *Remote Sens. Environ.* 258. doi:10.1016/j.rse.2021.112366.

Pahlevan, N., Smith, B., Alikas, K., Anstee, J., Barbosa, C., Binding, C., et al. (2022). Simultaneous retrieval of selected optical water quality indicators from Landsat-8, Sentinel-2, and Sentinel-3. *Remote Sens. Environ.* 270. doi:10.1016/j.rse.2021.112860.

Pavelsky, T. M., and Smith, L. C. (2008). RivWidth: A software tool for the calculation of river widths from remotely sensed imagery. *IEEE Geosci. Remote Sens. Lett.* 5, 70–73.

Petley, D. (2021). Catoca mine in Angola – using satellite imagery to understand recent events. *Landslide Blog*. Available at: https://blogs.agu.org/landslideblog/2021/09/06/catoca-mine-in-angola-using-satellite-imagery-to-understand-recent-events/.

QGIS Development Team (2022). QGIS Geographic Information System. Available at: QGIS Association [Accessed February 9, 2022].

Queiroz, H. M., Nóbrega, G. N., Ferreira, T. O., Almeida, L. S., Romero, T. B., Santaella, S. T., et al. (2018). The Samarco mine tailing disaster: A possible time-bomb for heavy metals contamination? *Sci. Total Environ.* 637–638, 498–506. doi:10.1016/j.scitotenv.2018.04.370.

R Core Team (2018). R: A Language and Environment for Statistical Computing.

Rana, N. M., Ghahramani, N., Evans, S. G., McDougall, S., Small, A., and Take, W. A. (2021). Catastrophic mass flows resulting from tailings impoundment failures. *Eng. Geol.* 292, 106262. doi:10.1016/j.enggeo.2021.106262.

Rasmussen, P. P., Gray, J. R., Glysson, G. D., and Ziegler, A. C. (2009). “Guidelines and procedures for computing time-series suspended-sediment concentrations and loads from in-stream turbidity-sensor and streamflow data: Techniques and Methods 3–C4,” in *U. S. Geological Survey Tehcniques and Methods Book 3, Applications of Hydraulics Section C, Sediment and Erosion Techniques* (Reston, Virginia: U. S. Geological Survey), 53.

Reichl, C., Schatz, M., and Zsak, G. (2020). World Mining Data 2020. Vienna: Federal Ministry of Agriculture, Regions and Tourism, Republic of Austria.

República de Angola (2011). Decreto Presidencial n. 261/11 de 6 de Outubro. Regulamento sobre a qualidade da água. República da Angola: Diário da República, I Série, No. 193.

Rico, M., Benito, G., and Díez-Herrero, A. (2008). Floods from tailings dam failures. *J. Hazard. Mater.* 154, 79–87. doi:10.1016/j.jhazmat.2007.09.110.

Roca, M., Murphy, A., Walker, L., and Vallesi, S. (2019). A review of the risks posed by the failure of tailings dams. HR Wallingford.

Roche, C., Thygesen, K., and Baker, E. eds. (2017). *Mine Tailings Storage: Safety Is No Accident. UNEP Rapid Response Assessment. United Nations Environment Programme*. Nairobi and Arendal: United Nations Environment Programme and GRID-Arendal.

RTNC (2021). Briefing Pollution Kasai. Available at: https://www.pscp.tv/w/1vOxwEXQNVRGB [Accessed November 22, 2021].

Rudorff, N., Rudorff, C. M., Kampel, M., and Ortiz, G. (2018). Remote sensing monitoring of the impact of a major mining wastewater disaster on the turbidity of the Doce River plume off the eastern Brazilian coast. *ISPRS J. Photogramm. Remote Sens.* 145, 349–361. doi:10.1016/j.isprsjprs.2018.02.013.

S&P Global Market Intelligence (2021). SNL metals and mining database. Available at: https://www.spglobal.com/marketintelligence/en/campaigns/metals-mining [Accessed December 10, 2021].

Santos, J. J. (2021). Catoca - contaminação da água dos rios Lova,Chicapa e Cassai. Available at: https://www.youtube.com/watch?v=cOv2rAeMorc [Accessed March 28, 2022].

Sentinel Vision, and Visio Terra (2021). The largest Angolan diamond mine poisons Kasai river, DRC. Available at: https://www.sentinelvision.eu/gallery/html/59f7f8cfa0ef49bab141c4eb6f55aee4 [Accessed November 22, 2021].

Sheffield, J., Wood, E. F., Pan, M., Beck, H., Coccia, G., Serrat-Capdevila, A., et al. (2018). Satellite Remote Sensing for Water Resources Management: Potential for Supporting Sustainable Development in Data-Poor Regions. *Water Resour. Res.* 54, 9724–9758. doi:10.1029/2017WR022437.

Simón, M., Ortiz, I., García, I., Fernández, E., Fernández, J., Dorronsoro, C., et al. (1999). Pollution of soils by the toxic spill of a pyrite mine (Aznalcollar, Spain). *Sci. Total Environ.* 242, 105–115. doi:10.1016/S0048-9697(99)00378-2.

Sinergise (2022). Sentinelhub. EO Browser. Available at: https://apps.sentinel-hub.com/eo-browser/ [Accessed March 5, 2022].

Sociedade Mineira de Catoca Lda. (2021). Comunicado de Imprensa. Available at: https://www.catoca.com/catoca-descarta-presenca-de-metais-pesados-na-polpa-de-rejeitados-que-chegou-ao-rio-lova/ [Accessed November 22, 2021].

Sracek, O., Kříbek, B., Mihaljevič, M., Majer, V., Veselovský, F., Vencelides, Z., et al. (2012). Mining-related contamination of surface water and sediments of the Kafue River drainage system in the Copperbelt district, Zambia: an example of a high neutralization capacity system. *J. Geochemical Explor.* 112, 174–188. doi:10.1016/j.gexplo.2011.08.007.

Strydom, J. (2015). The effect of kimberlite weathering on the behaviour of waste material at Cullinan diamond mine , South Africa .

Swain, R., and Sahoo, B. (2017). Mapping of heavy metal pollution in river water at daily time-scale using spatio-temporal fusion of MODIS-aqua and Landsat satellite imageries. *J. Environ. Manage.* 192, 1–14. doi:https://doi.org/10.1016/j.jenvman.2017.01.034.

Syifa, M., Park, S. J., Achmad, A. R., Lee, C. W., Eom, J., and Eom, J. (2019). Flood mapping using remote sensing imagery and artificial intelligence techniques: A case study in Brumadinho, Brazil. *J. Coast. Res.* 90, 197–204. doi:10.2112/SI90-024.1.

Teixeira, D. B. de S., Veloso, M. F., Ferreira, F. L. V., Gleriani, J. M., and do Amaral, C. H. (2021). Spectro-temporal analysis of the Paraopeba River water after the tailings dam burst of the Córrego do Feijão mine, in Brumadinho, Brazil. *Environ. Monit. Assess.* 193. doi:10.1007/s10661-021-09218-4.

Telmer, K., and Stapper, D. (2007). Evaluating and monitoring small scale gold mining and mercury

use: Building a knowledge-base with satellite imagery and field work. *United Nations Ind. Dev. Organ. Victoria, BC, Canada*, 48.

The Siberian Times Reporter (2016). Stinking poisoned water flows towards Siberia from mining city Ridder in Kazakhstan. Available at: http://siberiantimes.com/ecology/others/news/n0671-stinking-poisoned-water-flows-towards-siberia-from-mining-city-ridder-in-kazakhstan/ [Accessed February 8, 2022].

Thompson, F., de Oliveira, B. C., Cordeiro, M. C., Masi, B. P., Rangel, T. P., Paz, P., et al. (2020). Severe impacts of the Brumadinho dam failure (Minas Gerais, Brazil) on the water quality of the Paraopeba River. *Sci. Total Environ.* 705, 1–6. doi:10.1016/j.scitotenv.2019.135914.

Towriss, D. (2013). Buying Loyalty : Zimbabwe ' s Marange Diamonds Buying Loyalty : Zimbabwe ' s Marange. 7070, 99–117.

TPA (2021a). Catoca - Descarta presença de matais pesados na àgua. Available at: https://www.youtube.com/watch?v=rsmYg7ama5E [Accessed March 28, 2022].

TPA (2021b). Poluição no Rio Lova: Direcção de Avaliação de Impactos Ambientais reage à denúncia da TPA. Available at: https://www.youtube.com/watch?v=vUTqM_ZH1Co [Accessed March 28, 2022].

TPA (2021c). Responsável Nega Registo de Mortes por Vazamento de Produtos Químicos. *Noticias*. Available at: https://www.tpa.ao/ao/noticias/responsavel-nega-registo-de-mortes-por-vazamento-de-produtos-quimicos/ [Accessed March 28, 2022].

Tshamala, A. K., Musala, M. K., Kalenga, G. K., and Mumapanda, H. D. wa (2021). Assessment of Surface Water Quality in Kakanda: Detection of Pollution from Mining Activities. *J. Environ. Prot. (Irvine,. Calif).* 12, 561–570. doi:10.4236/jep.2021.129035.

Tshimanga, R. M. (2012). Hydrological uncertainty analysis and scenario-based streamflow modelling for the Congo River Basin. 324.

UNECE (2014). Safety guidelines and good practices for tailings management facilities. United Nations Economic Commission for Europe.

US National Park Service (2022). World Physical Map. *ArcGIS REST Serv. Dir.* Available at: https://server.arcgisonline.com/ArcGIS/rest/services/World_Physical_Map/MapServer/tile/%7Bz%7D/%7By%7D/%7Bx%7D [Accessed March 22, 2022].

Van der Walt, S., Schönberger, J. L., Nunez-Iglesias, J., Boulogne, F., Warner, J. D., Yager, N., et al. (2014). scikit-image: image processing in Python. *PeerJ* 2, e453.

Vanhellemont, Q. (2019). Adaptation of the dark spectrum fitting atmospheric correction for aquatic applications of the Landsat and Sentinel-2 archives. *Remote Sens. Environ.* 225, 175–192. doi:10.1016/j.rse.2019.03.010.

Vanhellemont, Q. (2020). Sensitivity analysis of the dark spectrum fitting atmospheric correction for metre- and decametre-scale satellite imagery using autonomous hyperspectral radiometry. *Opt. Express* 28, 29948. doi:10.1364/oe.397456.

Vanhellemont, Q. (2021). ACOLITE User Manual. Brussels: Royal Belgian Institute of Natural Sciences (RBINS).

Vanhellemont, Q., and Ruddick, K. (2018). Atmospheric correction of metre-scale optical satellite data for inland and coastal water applications. *Remote Sens. Environ.* 216, 586–597. doi:10.1016/j.rse.2018.07.015.

VoA Português (2021a). “Catástrofe ambiental” causada por rotura em sistema da mina de diamantes

de Catoca. Available at: https://www.voaportugues.com/a/catástrofe-ambiental-causada-por-rotura-em-sistema-da-mina-de-diamantes-de-catoca/6014262.html [Accessed March 28, 2022].

VoA Português (2021b). Catoca diz que testes confirmam que alegações da República Democrática do Congo não são verdade. Available at: https://www.voaportugues.com/a/catoca-diz-que-testes-confirmam-que-alegações-da-república-democrática-do-congo-não-são-verdade/6278187.html [Accessed March 28, 2022].

Wang, Z., Liu, J., Li, J., Meng, Y., Pokhrel, Y., and Zhang, H. (2021). Basin-scale high-resolution extraction of drainage networks using 10-m Sentinel-2 imagery. *Remote Sens. Environ.* 255, 112281. doi:10.1016/j.rse.2020.112281.

Warren, M. A., Simis, S. G. H., Martinez-Vicente, V., Poser, K., Bresciani, M., Alikas, K., et al. (2019). Assessment of atmospheric correction algorithms for the Sentinel-2A MultiSpectral Imager over coastal and inland waters. *Remote Sens. Environ.* 225, 267–289. doi:10.1016/j.rse.2019.03.018.

Wickham, H., Chang, W., Henry, L., Pedersen, T. L., Takahashi, K., Wilke, C., et al. (2019). ggplot2: Elegant Graphics for Data Analysis. Available at: https://ggplot2.tidyverse.org [Accessed October 15, 2020].

WISE Uranium Project (2022). Chronology of major tailings dam failures. Available at: https://www.wise-uranium.org/mdaf.html [Accessed February 9, 2022].

Zaitch, D., and Gómez, L. G. (2015). “Mining as state-corporate crime: The case of AngloGold Ashanti in Colombia,” in *The Routledge international handbook of the crimes of the powerful* (Routledge), 406–418.

Zeng, C., Bird, S., Luce, J. J., and Wang, J. (2015). A natural-rule-based-connection (NRBC) method for river network extraction from high-resolution imagery. *Remote Sens.* 7, 14055–14078.

Zhang, T. Y., and Suen, C. Y. (1984). A fast parallel algorithm for thinning digital patterns. *Commun. ACM* 27, 236–239.

Appendix

Suppl.-Table 1 List of coordinates of the virtual stations in Tshikapa River close to Catoca mine

Virtual Station	Longitude [degrees]	Latitude [degrees]	Distance to Lova River Inflow [m]	Dates manually removed
Upstream	20.363238	-9.334211	-5251	23.11.2018
Downstream	20.363316	-9.291250	4604	09.10.2018, 24.10.2019

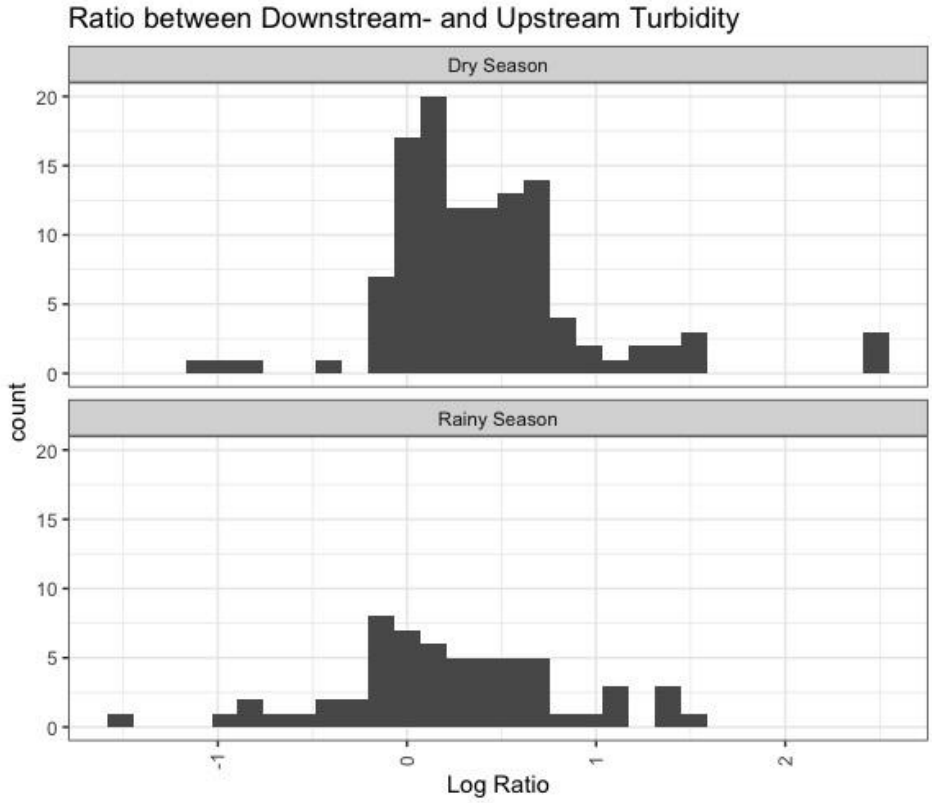

Suppl.-Figure 1 Histogram of point- to- point ratios of turbidity values between up - and downstream of virtual stations "wide" from Figure 7. In logarithmic scale.

Suppl.-Table 2 Mines operating currently close to Tshikapa River, extract from SNL database (S&P Global Market Intelligence, 2021)

Mine Name	Current Stage	Current Status	Latitude	Longitude
Catoca	Operating	Active	-9.39889	20.30083
Kamachia-Kamajiku	Limited Production	Inactive	-8.94671	20.47628
Calonda	Operating	Active	-8.515	20.543
Canvuri	Operating	Active	-8.963	20.423
Tchegi	Operating	Active	-9.12	20.35
Yetwene	Operating	Care And Maintenance	-8.29458	20.5082

Suppl.-Table 3 Calculations propagation speed of pollution front based on visual identification of pollution front on Sentinel-2 imagery (Sinergise, 2022)

Date	Latitude	Longitude	Pollution front [km]	Distance Lova Inlet [km]	Time span to previous [s]	Speed [m s^{-1}]
25.07.21 08:36:01	-9.128601	20.344405	83.106	60.4	**76249.9**	na
30.07.21 08:35:59	-6.939499	20.621618	425.4	402.7	431998	0.792
04.08.21 08:36:01	-4.622282	20.942001	759.5	736.8	432002	0.773
07.08.21 08:46:01	-3.939503	19.428108	977.3	954.6	259800	0.838
10.08.21 08:56:01	-3.322016	17.712536	1193.2	1170.5	259800	0.831
Lova Inlet to Tshikapa [km]	41.3				Arithmetic mean	0.809
Distance Lova to Tshikapa River [km]	18.6				Median	0.812
Start Pollution Front Catoca Mine	**24.07.21 11:51:56**					
Arrival Pollution Front Congo River	13.08.21 13:34:09					
Total distance to Congo River [km]	1402.5					
Travel time (days)	20.01					